Exosomal circ0000549 promotes MNNG-induced gastric cancer through miR-15b-5p/KIF1B

ZHAOFENG LIANG[1,2*], ZIHAN GAO[1,2*], YUE ZHANG[2], JIAJIA SONG[2], HUI QIAN[1,2] and XUEZHONG XU[1]

[1]Wujin Institute of Molecular Diagnostics and Precision Cancer Medicine of Jiangsu University, Wujin Hospital Affiliated with Jiangsu University, Changzhou, Jiangsu 213017, P.R. China; [2]Jiangsu Key Laboratory of Medical Science and Laboratory Medicine, School of Medicine, Jiangsu University, Zhenjiang, Jiangsu 212013, P.R. China

Received August 20, 2025; Accepted February 12, 2026

DOI: 10.3892/ijmm.2026.5785

Abstract. Accumulating evidence indicates that environmental exposures, particularly to nitrites, play a critical role in the initiation and progression of gastric cancer (GC). During carcinogenesis, exosomes act as key mediators of intercellular communication. Exosomes derived from N-methyl-N'-nitro-N-nitrosoguanidine (MNNG)-induced malignantly transformed GES-1 cells (TGES-1), as well as serum exosomes from gastric cancer patients with a history of high nitrite exposure, were found to influence normal cells and promote GC initiation. The present study established a malignant transformation model and applied bioinformatics analyses to screen and validate candidate circRNAs. A series of functional and mechanistic experiments were performed to elucidate the regulatory role of exosomes in GC progression. Circ0000549 was markedly upregulated in MNNG-exposed GES-1 cells, their derived exosomes and serum exosomes from patients with GC. Further investigations revealed that circ0000549 overexpression enhanced GES-1 cell malignant features, while also modulating epithelial-mesenchymal transition and stemness-related properties. Nude mouse experiments demonstrated that circ0000549, carried by malignantly transformed exosomes, plays a crucial role in MNNG-induced gastric carcinogenesis. Mechanistically, miR-15b-5p was identified as a potential target of circ0000549. Circ0000549 functioned as a sponge for miR-15b-5p, leading to increased KIF1B expression and subsequent activation of the PI3K/AKT signaling pathway. Collectively, these findings reveal that exosomal circ0000549 promotes malignant transformation of GES-1 cells through the miR-15b-5p/KIF1B/PI3K/AKT axis. Exosomal circ0000549 may serve as a promising biomarker for GC diagnosis and prognosis, highlighting its potential as a target for future therapeutic investigation.

Correspondence to: Professor Xuezhong Xu, Wujin Institute of Molecular Diagnostics and Precision Cancer Medicine of Jiangsu University, Wujin Hospital Affiliated with Jiangsu University, 2 Yongning North Road, Changzhou, Jiangsu 213017, P.R. China
E-mail: xuxuezhong@wjrmyy.cn

Professor Zhaofeng Liang, Jiangsu Key Laboratory of Medical Science and Laboratory Medicine, School of Medicine, Jiangsu University, 301 Xuefu Road, Zhenjiang, Jiangsu 212013, P.R. China
E-mail: liangzhaofeng@ujs.edu.cn

*Contributed equally

Key words: gastric cancer, exosome, Circ0000549, chemical carcinogenesis, N-methyl-N'-nitro-N-nitrosoguanidine, microRNA 15b-5p

Introduction

Gastric cancer (GC) is the fifth most frequently diagnosed malignancy worldwide and represents the fourth leading cause of cancer-related mortality (1,2). Precancerous lesions of GC refer to pathological alterations of the gastric mucosa that exhibit a high propensity for malignant transformation, involving multiple risk factors and multistep cellular changes (3). In-depth investigation of these precancerous lesions is essential for identifying key mechanisms underlying gastric carcinogenesis and provides critical evidence for early prevention and effective therapeutic intervention. Although advances in early screening and diagnostic technologies have been achieved in recent years, most patients with GC are still diagnosed at advanced stages of the disease (4,5). Numerous studies have shown that dietary factors play a significant role in the development of gastrointestinal malignancies; however, reliable early diagnostic biomarkers remain poorly defined (6,7). N-methyl-N'-nitro-N-nitrosoguanidine (MNNG), composed primarily of N-nitrosamines and N-nitrosamides, is a widely distributed environmental chemical mutagen and carcinogen (8,9). MNNG can form adducts with biological macromolecules, including DNA and proteins (10). It has been demonstrated that MNNG can induce precancerous lesions, tumor formation and malignant cellular transformation in animal models. For instance, MNNG exposure can lead to chronic atrophic gastritis, esophageal cancer and malignant transformation of normal intestinal epithelial cells in rats (11,12). Consequently, MNNG is commonly employed as an experimental agent to model nitroso compound-induced precancerous transformation of gastric mucosal cells (13,14). Previous studies have indicated that MNNG exposure activates multiple oncogenic signaling pathways, including NF-κB (15),

Wnt/β-catenin (16) and PI3K/Akt/mTOR (14). However, research focusing on the underlying molecular mechanisms remains limited.

Circular RNAs (circRNAs) constitute a class of non-coding RNA molecules characterized by covalently closed loop structures, which confer greater stability compared with linear RNAs. Initially, circRNAs were considered byproducts of aberrant splicing events during transcription (17,18). However, accumulating evidence has shown that circRNAs are predominantly generated through back-splicing, a process in which exons from precursor mRNAs are ligated to form circular transcripts (19). CircRNAs are widely expressed and exhibit high abundance, remarkable stability and strong tissue- and disease-specific expression patterns (20). An increasing number of studies have revealed that circRNAs play diverse regulatory roles in both physiological and pathological processes, including cancer initiation and progression. For example, Lin *et al* (21) identified a novel circRNA, circTFRC, which is markedly upregulated in GC tissues and cell lines. Elevated plasma levels of circTFRC were closely associated with tumor size and metastasis and mechanistically, circTFRC promotes GC malignancy by impairing ferroptosis susceptibility. In another study, circ_0005927 was shown to suppress proliferation, colony formation, invasion and epithelial-mesenchymal transition (EMT) in GC cells by sponging miR-570-3p and upregulating forkhead box O3 (FOXO3), suggesting that the circ_0005927/miR-570-3p/FOXO3 axis represents a potential therapeutic target for GC (22). Collectively, these findings highlight the critical roles of circRNAs in GC. Nevertheless, a large number of circRNAs remain uncharacterized and their biological functions and underlying mechanisms in GC require further investigation.

The tumor microenvironment (TME) is a highly complex and dynamic system formed through interactions among cancer cells, stromal cells, immune cells and other surrounding components (23). Exosomes are a subtype of extracellular vesicles with diameters ranging from 30-200 nm. They are released by nearly all cell types and have emerged as promising biomarkers for the detection and diagnosis of various diseases (24,25). Within the TME, exosomes function as critical mediators of intercellular communication, acting as 'membrane messengers' that transmit biological signals between cells (26). However, the roles and regulatory mechanisms of exosome-derived circRNAs in malignant cellular transformation remain largely unexplored.

The current study investigated the effects of long-term MNNG exposure and MNNG-induced exosomes on the migratory, proliferative and invasive capacities of normal GES-1 cells. By analyzing data from the Gene Expression Omnibus (GEO) database (https://www.ncbi.nlm.nih.gov/geo/; accessed in May 2023), has_circ-0000549 (circ0000549, circSRSF5) was identified as a candidate circRNA with markedly elevated expression in GC tissues and plasma samples. Subsequent validation confirmed that circ0000549 expression was markedly increased in GES-1 cells following prolonged MNNG exposure. Moreover, circ0000549 packaged within exosomes released from MNNG-induced malignantly transformed cells could be transferred to neighboring normal gastric epithelial cells. Functionally, exosomal circ0000549 enhanced invasion, migration and proliferation, while promoting stemness and EMT in normal GES-1 cells through the miR-15b-5p/KIF1B/PI3K/AKT signaling axis. These findings provide novel insights into the mechanisms underlying MNNG-induced gastric carcinogenesis.

Materials and methods

Cell culture. The human gastric epithelial cell line GES-1 was obtained from Shanghai Enzyme Linked Biotechnology Co., Ltd. Cells were cultured in Dulbecco's Modified Eagle's Medium (DMEM; Dalian Meilun Biology Technology Co., Ltd.) enriched with 10% fetal bovine serum (FBS; Gibco; Thermo Fisher Scientific, Inc.) and maintained at 37˚C in a humidified incubator containing 5% CO_2. To establish a malignant transformation model, GES-1 cells were chronically exposed to MNNG. Based on preliminary cell survival assays, MNNG concentrations of 0.5 and 1 μmol/l were selected for subsequent experiments. When cells reached 80-90% confluence, they were washed twice with phosphate-buffered saline (PBS), digested with trypsin and centrifuged at 35 x g at room temperature for 5 min. Cells were then passaged at a ratio of 1:3 and cultured in 8 ml DMEM containing 10% FBS under standard conditions (37˚C, 5% CO_2), with the culture medium replaced daily. On the day following cell passage, a 0.01 mol/l MNNG stock solution was diluted with fresh DMEM to achieve final MNNG concentrations of 0, 0.5 and 1 μmol/l. Cells were continuously treated for ~30 passages to induce malignant transformation and aliquots of cells were cryopreserved at passages 5, 10, 25 and 30 for subsequent analyses. The malignantly transformed GES-1 cells were designated as TGES-1.

Bioinformatics analysis of differentially expressed circRNAs. Bioinformatic screening was performed using two publicly available GC-related circRNA datasets (GSE89143 and GSE93541) from the GEO database. Differential expression analysis was conducted using the GEO2R online tool (https://www.ncbi.nlm.nih.gov/geo/geo2r/), which is based on the limma R package (Version 3.54.0; https://bioconductor.org/packages/limma/) for data normalization and statistical evaluation. CircRNAs with an adjusted $P<0.05$ and a $\log_2$ (fold change) >1 were defined as markedly differentially expressed. From each dataset, the top 249 circRNAs meeting these criteria were selected for subsequent intersection analysis. A Venn diagram was generated using the jvenn online tool (https://jvenn.toulouse.inrae.fr/app/index.html) to identify circRNAs shared between the two datasets. Expression data corresponding to the overlapping circRNAs were then extracted from both datasets and converted into circBase ID format for standardization. Finally, a heatmap visualizing the expression patterns of these shared circRNAs across different samples was constructed using TBtools software (version 2.025, https://github.com/CJ-Chen/TBtools/releases). Based on these analyses, the candidate differentially expressed circRNAs were further validated and selected for downstream experimental investigation.

CircInteractome-based prediction of circ0000549-AGO2 binding interaction. The potential binding of circ0000549 to Argonaute 2 (AGO2) was predicted using the online

bioinformatics tool CircInteractome (https://circinteractome.nia.nih.gov/). The full nucleotide sequence of circ0000549 was input into the analysis module of the database, with the default algorithm parameters retained for the AGO2 binding site prediction. The prediction was performed based on data integrated in the database, and the results were filtered to identify the reliable binding motifs of circ0000549 to AGO2, so as to confirm the potential interaction between circ0000549 and AGO2.

Target gene prediction for miR-15b-5p. Potential target genes of miR-15b-5p were predicted using five independent bioinformatics algorithms: miRDB (version 1.0; https://mirdb.org/), DIANA microT-CDS (version 5.0; https://www.microrna.gr/microt_webserver/), miRWalk (version 2.0; http://mirwalk.umm.uni-heidelberg.de/), StarBase (version 3.0, StarBase or ENCORI: Decoding the Encyclopedia of RNA Interactomes, https://rnasysu.com/encori/) and TargetScan (version 8.0; https://www.targetscan.org/vert_80/). All predictions were performed using the default parameters and score thresholds provided by each database. All genes predicted by each tool were collected without applying additional filters. The predicted gene sets were then intersected and genes identified by at least three of the five algorithms were defined as high-confidence target candidates. Based on this intersection analysis, six candidate target genes were screened and further subjected to multiple validation assays to determine the bona fide target molecule.

Definition of high nitrite compound exposure. Patients were categorized into the 'high nitrite exposure' group based on a combined evaluation of dietary history and relevant biomarkers.

Dietary Assessment: Patients were required to have a confirmed history of long-term and regular consumption of foods rich in N-nitroso compounds or their precursors. Dietary intake was determined via a structured questionnaire, focusing on the consumption of preserved foods, processed meats and high-salt diets.

Biomarker Assessment: Serum levels of nitrosation-related metabolites, including N-nitrosoproline, were quantified using liquid chromatography-tandem mass spectrometry (LC-MS/MS). Levels exceeding established reference ranges were defined as indicative of high nitrite exposure.

Liquid chromatography-tandem mass spectrometry (LC-MS/MS) quantification of serum N-nitrosoproline. Serum levels of N-nitrosoproline were determined by LC-MS/MS. Aliquots of serum underwent protein precipitation with cold acetonitrile containing a stable isotope-labeled internal standard. The processed samples were analyzed using an Acquity UPLC system (Waters Corporation) equipped with an HSS T3 column. A gradient elution was applied with mobile phases consisting of 0.1% formic acid in water and acetonitrile. Detection was performed on a triple quadrupole mass spectrometer operating in positive electrospray ionization mode, with quantification achieved via multiple reaction monitoring (MRM). The MRM transitions monitored were m/z 157.1 to m/z 74.1 for N-nitrosoproline and m/z 158.1 to m/z 75.1 for the internal standard. The mass spectrometer parameters were set as follows: nitrogen gas temperature 500˚C, nebuliser pressure 7.0 psi, and desolvation gas flow rate 800 l/h. A threshold corresponding to the 95th percentile of levels measured in a reference cohort with low dietary nitrite intake defined the high-exposure group.

Patients and clinical specimens. Patients with GC (n=40) with a documented history of high nitrite exposure were randomly recruited from the Affiliated Hospital of Jiangsu University. All patients were definitively diagnosed by histopathological examination prior to surgical intervention and had not received any anticancer treatment before sample collection. Written informed consent was obtained from each participant and the study protocol was approved by the Medical Ethics Committee of Jiangsu University (ethics approval no. 2023182). Peripheral blood samples were collected from both patients with GC and corresponding normal controls. Plasma was separated from whole blood by centrifugation at 2,000 x g for 10 min at 4˚C and stored for subsequent analyses. The inclusion criteria for patients were: Being newly diagnosed and histopathologically confirmed with primary gastric adenocarcinoma; age between 25 and 65 years; having no history of other malignancies; receiving no prior chemotherapy, radiotherapy, or targeted therapy before sample collection; availability of complete clinical and follow-up data; and for the 'high nitrite exposure' subgroup, meeting the predefined criteria of combined dietary history assessment and serum N-nitrosoproline level as described in the 'Definition of high nitrite compound exposure' section. Exclusion criteria comprised: Patients with recurrent or metastatic gastric cancer at initial diagnosis; patients with severe concurrent systemic infections, autoimmune diseases, or other major organ dysfunction; pregnant or lactating women; and those with incomplete dietary history or insufficient serum sample for biomarker analysis. The demographic characteristics of the patients were shown in Table SI. All patients provided written informed consent for the use of their samples in scientific research. Samples were collected between March 2023 and March 2024 in accordance with the approved protocol.

Exosome experiments. Cells were cultured in 10-cm culture dishes until ~50% confluence. The culture medium was then replaced with fresh medium enriched with 10% exosome-depleted FBS following two washes with PBS. After 48 h of incubation at 37˚C, the conditioned medium was collected and subjected to sequential centrifugation as previously described (27,28) for exosome isolation. Briefly, the conditioned medium was centrifuged at 2,000 x g at 4˚C for 10 min to remove intact cells, followed by centrifugation at 10,000 x g at 4˚C for 30 min to clear cell debris and then ultracentrifuged at 100,000 x g at 4˚C for 2 h (repeated once). Freshly isolated exosomes were resuspended in PBS, filtered through a 0.2-μm membrane and stored at -80˚C until further use. Exosomes were characterized and identified using a combination of western blot analysis, nanoparticle tracking analysis (NTA) and transmission electron microscopy (TEM). For TEM analysis (conducted by Zhenjiang Danyang Zhuanbo Testing Technology Co., Ltd.), exosomes were fixed with glutaraldehyde, dropped onto copper grids for 3 min adsorption (residual liquid blotted with filter paper), negatively stained with phosphotungstic acid (pH=6.8) at room temperature for 1 min,

dried under incandescent light, and then observed and imaged. For NTA, the NanoSight instrument (Waters Corporation) was preheated for ~30 min after power-on, cleaned with purified water, and exosomes were diluted to an appropriate concentration with purified water, mixed thoroughly, injected via a 1 ml syringe, and analyzed with relevant parameters recorded. In addition, plasma-derived exosomes from human samples were isolated using the ExoQuick Plasma Prep and Exosome Precipitation Kit (System Biosciences, LLC).

DiL-labeled exosome uptake assay. Coverslips were attached to the bottom of 12-well plates with medium. GES-1 cells in logarithmic phase were trypsinized and seeded onto coverslips at $6x10^3$ cells/well, then incubated at 37˚C with 5% CO_2. Exosomes were labeled with DiL dye (MilliporeSigma; 1:1,000 dilution) for 30 min at 37˚C in the dark, centrifuged at 3,000 x g for 15 min, and filtered through a 0.22 μm filter (MilliporeSigma). Labeled exosomes were added to adherent cells and cultured for 24 h at 37˚C with 5% CO_2. Cells were rinsed twice with PBS, fixed with 4% paraformaldehyde for 30 min at room temperature, and washed three times with PBS at room temperature. Nuclei were stained with DAPI (MilliporeSigma) for 20 min at room temperature, followed by three PBS washes (5 min each). Coverslips were mounted with glycerol and sealed, then imaged using a confocal laser scanning microscope.

RNA extraction and reverse transcription-quantitative (RT-q) PCR. Total RNA was extracted from $2x10^7$ GES-1 and TGES-1 cells using RNA isolator Total RNA Extraction Reagent (TRIzol® method; Vazyme Biotech Co., Ltd.) according to the manufacturer's instructions. Complementary DNA (cDNA) was synthesized using the HiScript QRT SuperMix for qPCR kit (Vazyme Biotech Co., Ltd.) following the manufacturer's standard protocol. RT-qPCR was subsequently performed on an Applied Biosystems QuantStudio 3 Real-Time PCR System (Thermo Fisher Scientific, Inc.) using SYBR Green PCR Master Mix (Vazyme Biotech Co., Ltd.) according to the manufacturer's recommendations. The PCR cycling conditions were as follows: pre-denaturation at 95˚C for 5 min, followed by 40 cycles of denaturation at 95˚C for 20 sec, annealing at 60˚C for 30 sec and extension at 72˚C for 20 sec. Relative gene expression levels were calculated using the $2^{-\Delta\Delta Cq}$ method as previously described (29), with GAPDH used as the normalizer. All experiments were independently replicated three times. The primers used in RT-qPCR were shown in Table SII.

Cell counting kit-8 (CCK8) assay. Logarithmically growing cells were seeded into 96-well plates at a density of $1x10^3$ cells per well. Cell viability was assessed at 24, 48, 72 and 96 h after seeding. At each time point, 10 μl of CCK-8 reagent was added to each well, followed by incubation for an additional 3 h at 37˚C. Absorbance was measured at 450 nm using a microplate reader. All experiments were performed in triplicate.

Colony formation assay. Logarithmically growing cells were seeded into 3.5-cm culture dishes at a density of $1x10^3$ cells per dish. The cells were cultured for 7-14 days until visible colonies formed. The culture medium was then discarded and cells were gently washed twice with PBS, fixed with 4% paraformaldehyde at room temperature for 30 min and stained with crystal violet at room temperature for 15 min. After washing, colonies were counted and images captured.

Transwell assay. Logarithmically growing cells were harvested, resuspended in serum-free DMEM and seeded into the upper chambers of 24-well Transwell inserts at a density of $3x10^4$ cells per well. For invasion assays, the inserts were pre-coated with 50 μl of Matrigel diluted 1:4 in serum-free DMEM and incubated at 37˚C with 5% CO_2 for 1 h to allow solidification, whereas uncoated inserts were used for migration assays. Complete culture medium containing 10% FBS was added to the lower chambers. After 24 h of incubation at 37˚C, non-migrated or non-invaded cells on the upper surface of the membrane were removed. Cells on the lower surface were fixed with paraformaldehyde at room temperature for 15 min and stained with crystal violet at room temperature for 10 min. Migrated or invaded cells were counted under a light microscope at 10x magnification.

Western blotting. Total protein was extracted from cells using RIPA lysis buffer (Thermo Fisher Scientific, Inc.). Protein concentration was determined using a BCA protein assay kit (Vazyme Biotech Co., Ltd.). Equal amounts of protein (50-60 μg) were loaded per lane separated by 10% sodium dodecyl sulfate-polyacrylamide gel electrophoresis and transferred onto polyvinylidene fluoride (PVDF) membranes. The membranes were blocked with 5% skimmed milk for 1 h at room temperature and incubated overnight at 4˚C with primary antibodies against N-cadherin (Cell Signaling Technology, Inc; cat. no. 13116S; dilution: 1:1,000), E-cadherin (Cell Signaling Technology, Inc; cat. no. 3195S; dilution: 1:1,000), PCNA (Cell Signaling Technology, Inc.; cat. no. 13110S; dilution: 1:1,000), Nanog (Cell Signaling Technology, Inc.; cat. no. 4903S; dilution: 1:1,000), OCT4 (Cell Signaling Technology, Inc; cat. no. 2750; dilution: 1:1,000), Lin28 (Cell Signaling Technology, Inc.; cat. no. 8706S; dilution: 1:1,000), SOX2 (Cell Signaling Technology, Inc; cat. no. 23064S; dilution: 1:1,000), Vimentin (Cell Signaling Technology, Inc.; cat. no. 5741S; dilution: 1:1,000), HSP70 (Cell Signaling Technology, Inc.; cat. no. 4872S; dilution: 1:1,000), Alix (Cell Signaling Technology, Inc.; cat. no. 92880S; dilution: 1:1,000), TSG101 (Proteintech, Inc; cat. no. 28283-1-AP; dilution: 1:1,000), Calnexin (Cell Signaling Technology, Inc.; cat. no. 2679S; dilution: 1:1,000), KIF1B (Abcam; cat. no. ab72108; dilution:1:1,500) and GAPDH (Bioworld Technology, Inc.; cat. no. BS65483M; dilution: 1:2,000). After washing with TBST containing 0.1% Tween-20, membranes were incubated with appropriate horseradish peroxidase-conjugated secondary antibodies (Signalway Antibody LLC; cat. no. L3012; dilution: 1:5,000). Protein bands were visualized using an enhanced chemiluminescence (ECL) detection system (Vazyme Biotech Co., Ltd.) and band intensities were quantified using ImageJ software (version 1.53k, National Institutes of Health).

In vivo xenograft experiments. Male nude mice (4-6 weeks old; weighing 18-22 g; SPF grade; n=3 per group; total n=24) were purchased from Shanghai SLAC Laboratory Animal Co., Ltd. All mice were housed under specific pathogen-free conditions at 22-25˚C and 50-60% humidity with a 12 h

light/dark cycle and randomly assigned to experimental groups. TGES-1 cells, GES-1 cells, TGES-1 cells treated with si-circ0000549-derived exosomes, or TGES-1 cells treated with exosomes derived from circ0000549-overexpressing cells combined with miR-15b-5p mimics were harvested by trypsinization and resuspended in PBS at a concentration of $5x10^7$ cells in 100 μl. The cell suspensions were then subcutaneously inoculated into the right flank of each mouse. Mice were observed daily for general health status and tumor growth was monitored weekly by caliper measurements. The following humane endpoints were predefined: Tumor volume >2,000 mm^3, ulceration or necrosis of the tumor, significant weight loss (>20% of body weight), or signs of severe distress (such as lethargy, hunched posture, impaired mobility). No animals reached these endpoints or succumbed prior to the scheduled endpoint.

The experiment lasted for 4 weeks post-inoculation. All animals were housed under standard conditions (12-h light/dark cycle; controlled temperature and humidity) with *ad libitum* access to food and water. To minimize distress, handling was performed gently and cage enrichment was provided. No analgesics or anesthetics were required during the tumor monitoring phase.

At the experimental endpoint, mice were sacrificed by cervical dislocation under deep anesthesia induced by intraperitoneal injection of sodium pentobarbital (80 mg/kg body weight). Mortality was confirmed by the absence of a heartbeat, cessation of breathing and loss of corneal reflex. Tumors were then excised, images captured and stored at -80˚C for subsequent analysis.

Plasmid transfection. To inhibit the expression of circ0000549 and KIF1B, specific small interfering RNAs (siRNAs) were synthesized and transfected into cells, while a non-targeting siRNA served as the negative control. miR-15b-5p expression was either enhanced or suppressed using miR-15b-5p mimics or inhibitors, respectively. The sequences of all siRNAs are in Table SIII. The siRNAs targeting circ0000549 and KIF1B were designed and synthesized by Shanghai GenePharma Co., Ltd. These siRNAs were designed based on the sequences of the target transcripts retrieved from the circBase (Version 0.1; https://www.circbase.org/) and NCBI GenBank database (Version Release 263.0; https://www.ncbi.nlm.nih.gov/genbank/) (circ0000549, accession number: NM_006925; KIF1B, accession number: accession numbers: NM_001365952.1).

Cells in the logarithmic growth phase were digested with trypsin, centrifuged at 35 x g for 5 min at room temperature, resuspended in complete medium, and seeded into 6-well plates for overnight incubation. After cell adhesion, the wells were washed twice with PBS, and 1.5 ml of Opti-MEM serum-free medium (Gibco; Thermo Fisher Scientific, Inc.) was added before the plates were returned to a 37˚C incubator. For transfection, 5 μl of Lipofectamine 2000 (Invitrogen; Thermo Fisher Scientific, Inc.) was mixed with 245 μl of Opti-MEM in the dark. In parallel, 5 μl of siRNA (final concentration: 50 nM) was diluted in 245 μl of Opti-MEM and incubated at room temperature for 5 min. The two solutions were then combined to form a 500 μl mixture, which was added to the cells and mixed gently. After incubation at 37˚C for 6 h, the medium was replaced with complete medium and cells were cultured for another 24-36 h before further experiments.

Generation of circ0000549 knockdown/overexpression stable cell lines. Cells in the logarithmic growth phase were trypsinized and seeded into 6-well plates ($3x10^4$ cells/well). After overnight culture, the medium was replaced with 2 ml of fresh medium containing 2 μg/ml polybrene and the appropriate volume of lentivirus, based on the predetermined multiplicity of infection (MOI). Following 24-h incubation, the lentivirus-containing medium was aspirated and replaced with complete medium. The optimal MOI was determined by assessing fluorescence intensity under a microscope and validating infection efficiency via RT-qPCR. The lentivirus used was a third-generation lentiviral expression system. For lentivirus production conducted by HANBIO Biotechnology Co., Ltd., 293T cells (ATCC) were transfected with lentiviral vector, packaging plasmid, and envelope plasmid at a mass ratio of 5:3:2 (total plasmid amount per 10 cm dish: 20 μg). Viral supernatants were harvested post-transfection, filtered and concentrated before supply. The optimal MOI for circ0000549 overexpression was 100. The lentiviruses for overexpression were designated as OE-NC and OE-circ549, while those for knockdown were designated as SH-NC and SH-circ549.

Subsequently, cells were infected at the optimal MOI and selected with 20 μg/ml puromycin. Stable cell pools were obtained after selection, indicated by fluorescence in >95% of adherent cells with minimal cell death. Successful circ0000549 knockdown or overexpression was confirmed by RT-qPCR.

Agarose gel electrophoresis. A 3% agarose gel was prepared by dissolving 1.8 g agarose powder (Invitrogen; Thermo Fisher Scientific, Inc.) in 60 ml of 0.5XTAE buffer (prepared from 50XTAE buffer; MilliporeSigma), followed by microwave heating. After solidification, the gel was placed in an electrophoresis tank and submerged with 0.5XTAE buffer. PCR products (1 μl) were mixed with loading buffer at a ratio of 5:1 and loaded into wells. Electrophoresis was carried out at 110 V until the marker migrated two-thirds of the gel length. The gel was stained with SYBR Safe (Invitrogen; Thermo Fisher Scientific, Inc.) and visualized using a gel imaging system (Bio-Rad Laboratories, Inc.).

RNA fluorescence in situ hybridization (FISH). A Cy3-labeled probe specifically targeting circ0000549 was synthesized by Shanghai GenePharma Co., Ltd. FISH was performed using a commercially available FISH kit (Shanghai GenePharma Co., Ltd.). Fluorescence signals were visualized and captured using a fluorescence microscope.

Dual-luciferase reporter assay. Plasmids containing wild-type (WT) or mutant (MUT) sequences of circ0000549, as well as miRNA mimics and corresponding control constructs, were synthesized by Shanghai GenePharma Co., Ltd. Cells were co-transfected with the aforementioned plasmids using Lipofectamine® 2000 Transfection Reagent (Invitrogen; Thermo Fisher Scientific, Inc.) according to the manufacturer's instructions. After 48 h of transfection, luciferase activity was measured using the Dual-Luciferase Reporter Assay System (Vazyme Biotech Co., Ltd.) strictly following the kit's protocol.

GeneCards database analysis. To predict potential signaling pathways associated with KIF1B, the GeneCards database (https://www.genecards.org/) was queried using 'KIF1B' as the search term. All signaling pathways listed in the 'Pathways' section of the KIF1B gene profile were retrieved. Pathways previously reported to be associated with cancer-related biological processes, including cell proliferation, apoptosis, migration and differentiation, were prioritized for further analysis. Based on their functional relevance to the cellular phenotypes examined in the present study, as well as their well-established involvement in tumor biology, the PI3K/AKT signaling pathway was selected for subsequent investigation. This selection was further supported by experimental validation performed in the present study.

In addition, other pathways predicted to be associated with KIF1B included Golgi-to-ER retrograde transport, vesicle-mediated transport, cytoskeletal signaling and response to elevated platelet cytosolic Ca^{2+} levels.

Immunohistochemistry. Formalin-fixed, paraffin-embedded tumor tissues obtained from nude mice were subjected to immunohistochemical staining. Tissues were fixed in 4% neutral buffered formalin (Sangon Biotech Co., Ltd.) for 24 h at room temperature, dehydrated through a graded ethanol series (70, 80, 90, 95, and 100% ethanol, 15 min each), cleared in xylene (twice for 15 min each), and embedded in paraffin wax. Sections (4 μm) were first deparaffinized and rehydrated using standard procedures. Antigen retrieval was performed by heating the sections in 0.01 M citrate buffer (pH 6.0) for 2 min. Endogenous peroxidase activity was blocked by incubation with 0.3% H_2O_2 for 10 min. Non-specific binding was then blocked with bovine serum albumin (BSA; MedChemExpress) for 30 min. Subsequently, the sections were incubated overnight at 4˚C with primary antibodies against Vimentin (Cell Signaling Technology, Inc; cat. no. 5741S; dilution:1:500) and Nanog (Cell Signaling Technology, Inc; cat. no. 4903S; dilution:1:500). After incubation with a biotinylated secondary antibody (Thermo Fisher Scientific, Inc.; cat. no. 31822; dilution: 1:1,000; conjugate: biotin), immunoreactivity was visualized using SABC detection system (Wuhan Boster Biological Technology, Ltd.) for 30 min at room temperature, followed by counterstaining with hematoxylin for 2 min at room temperature. Images were captured with a light microscope (Olympus BX53; Olympus Corporation) at 400x magnification.

Statistical analysis. All statistical analyses were performed with GraphPad Prism version 8.0 (Dotmatics). Data were analyzed utilizing either Student's t-test or one-way analysis of variance (ANOVA) followed by Bonferroni's post hoc test, as appropriate. $P<0.05$ was considered to indicate a statistically significant difference.

Results

MNNG induces malignant transformation of GES-1 cells. GES-1 cells were exposed to increasing concentrations of MNNG (0, 0.1, 0.5, 1, 2 and 5 μM) for 72 h. Cell viability assessment using the CCK-8 assay revealed that a statistically significant inhibitory effect was first observed at a concentration of 1 μM MNNG (Fig. 1A). Based on these results, 0.5 μM and 1 μM MNNG were selected for long-term exposure experiments to establish a malignant transformation model. GES-1 cells treated continuously with 1 μM MNNG for 30 passages were defined as malignantly transformed GES-1 cells (TGES-1). Morphological observation showed that prolonged MNNG exposure markedly altered the appearance of GES-1 cells, which gradually changed from a typical round or cobblestone-like morphology to a spindle-shaped or cord-like phenotype (Fig. 1B). To determine whether long-term MNNG exposure induced malignant transformation, a series of functional assays, including migration and invasion assays, cell proliferation assays and colony formation assays, were performed. The results demonstrated that GES-1 cells treated with 1 μM MNNG for 30 passages exhibited markedly enhanced proliferative capacity, as well as increased migration and invasion abilities (Fig. 1C-E). Furthermore, RT-qPCR and western blot analyses showed that the expression levels of mesenchymal markers and proliferation- and stemness-related proteins, including N-cadherin, Vimentin, PCNA, OCT4, SOX2, Lin28 and NANOG, were markedly upregulated in MNNG-induced GES-1 cells, whereas the epithelial marker E-cadherin was obviously downregulated (Fig. 1F and G).

In vivo tumorigenicity assays further confirmed the malignant transformation of TGES-1 cells. The incidence of xenograft tumors formed after subcutaneous injection of TGES-1 cells, was 100% (6/6 per group), whereas no tumors were observed in mice injected with control GES-1 cells (0/6; Fig. 1H). Collectively, these findings demonstrated that both *in vitro* and *in vivo* exposure to MNNG is sufficient to induce malignant transformation of normal GES-1 cells.

TGES-1 cells affects the biological characteristics of GES-1 cells via exosomes. Cancer cells are capable of inducing malignant alterations in surrounding normal cells within the TME. To investigate whether TGES-1 cells influenced the biological behavior of normal gastric epithelial cells, GES-1 and TGES-1 cells were co-cultured (Fig. 2A). The proliferative, migratory and invasive capacities of GES-1 cells before and after co-culture were evaluated using CCK-8 assays, colony formation assays and Transwell assays. The results showed that co-culture with TGES-1 cells clearly enhanced the proliferative ability of GES-1 cells. In addition, the migration and invasion capacities of GES-1 cells were markedly increased following co-culture (Fig. 2B-D). Moreover, the mRNA expression levels of EMT markers and stemness-associated genes were obviously upregulated (Fig. 2F and G).

Previous studies have demonstrated that cancer cells can modulate the malignant transformation of adjacent or distant normal epithelial cells through the secretion of exosomes (30,31). Based on this evidence, it was hypothesized that TGES-1 cells exert their effects on GES-1 cells via exosome-mediated communication. Exosomes were isolated from TGES-1 cells that had been continuously exposed to 1 μM MNNG for 30 passages (TGES-1-EX). The morphological features, particle size distribution and surface marker expression of TGES-1-EX were characterized using TEM, NTA and western blotting, respectively. TEM imaging revealed typical cup-shaped, double-membrane vesicles characteristic of exosomes (Fig. 2G). NTA analysis demonstrated that the mean particle diameters were 197.6 and 188.7 nm (Fig. 2H). Western

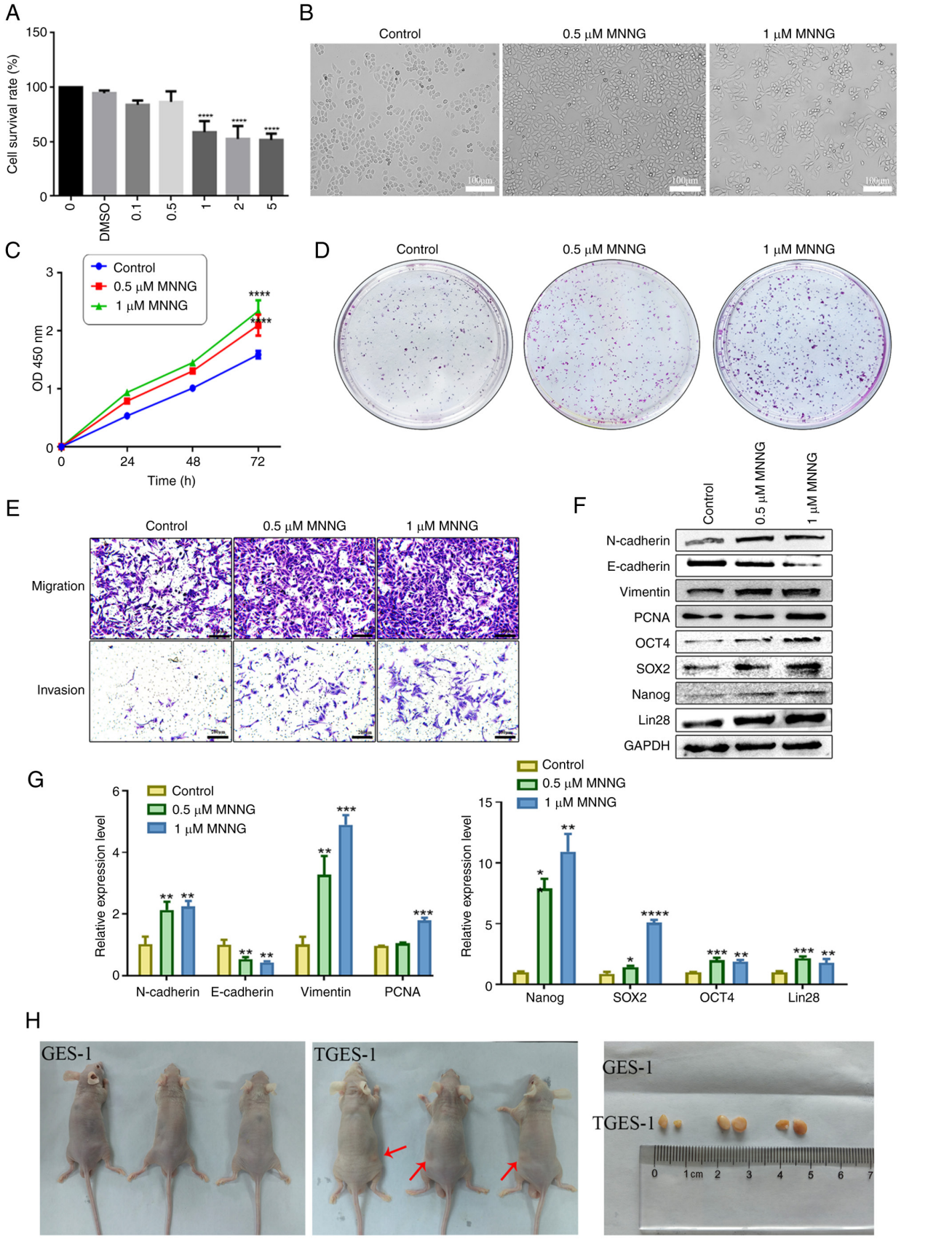

Figure 1. MNNG induces malignant transformation of GES-1 cells. (A) CCK8 assay results showing the survival rate of GES-1 cells after exposure to MNNG for 72 h. (B) Morphological alterations observed in GES-1 cells following exposure to MNNG for 30 generations. (C) CCK8 assay results demonstrating the proliferation of GES-1 cells after 30 passages following MNNG exposure. (D) Cloning efficiency of GES-1 cells treated with MNNG. (E) Migration and invasion capabilities of GES-1 cells after continuous MNNG treatment for 30 generations. (F) Western blot analysis of protein levels of EMT and stemness markers in MNNG-treated GES-1 cells. (G) RT-qPCR results showed the expression levels of EMT and stemness-related mRNA in MNNG-treated GES-1 cells. (H) Tumor size observed 4 weeks after injection of $5x10^7$ TGES-1 cells into nude mice. *P<0.05, **P<0.01, ***P<0.001, ****P<0.0001. MNNG, N-methyl-N'-nitro-N-nitrosoguanidine; EMT, epithelial-mesenchymal transition; RT-qPCR, reverse transcription-quantitative PCR.

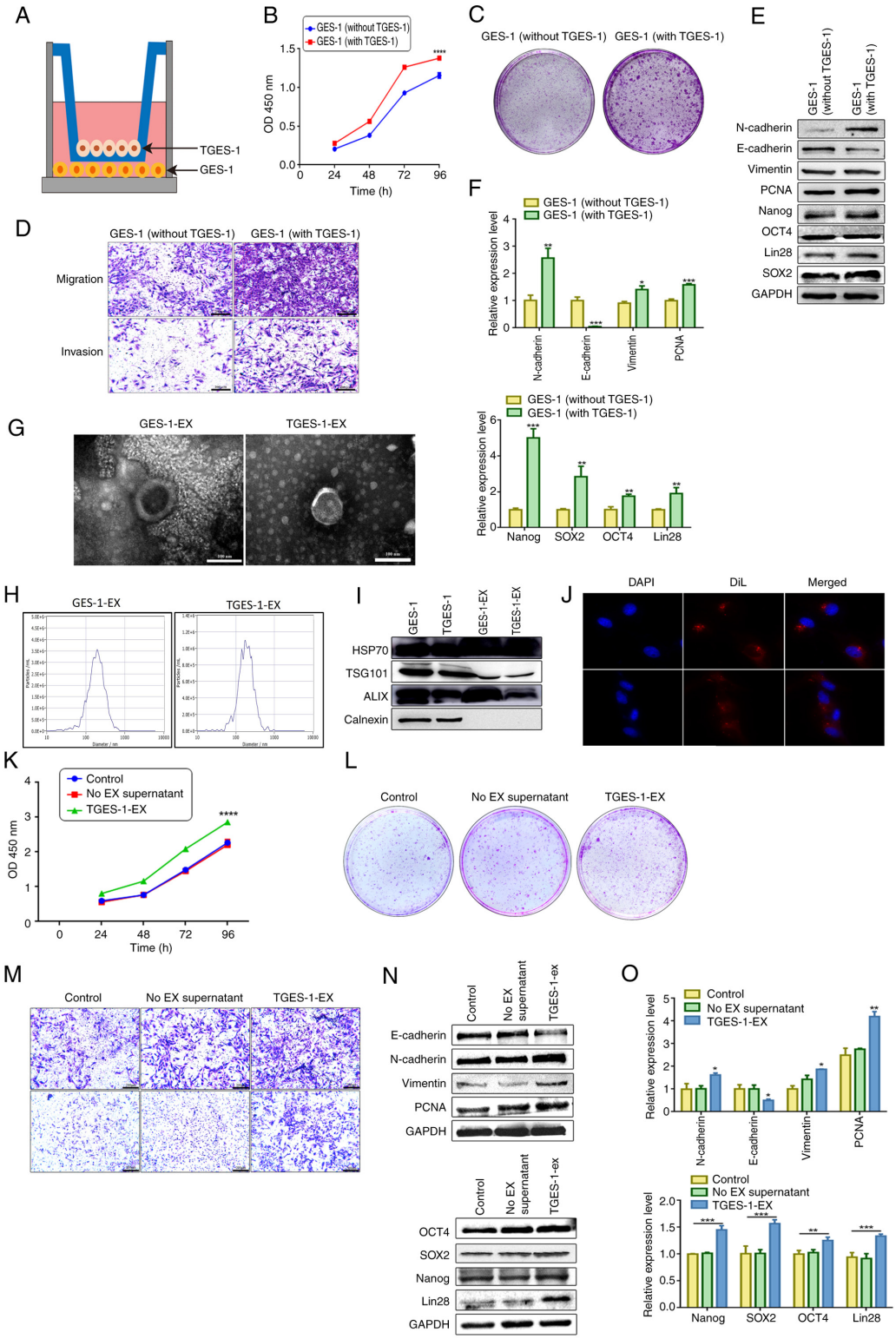

Figure 2. TGES-1 cells induce the biological changes of GES-1 cells through exosomes. (A) Schematic representation of GES-1 and TGES-1 cells in co-culture. (B) CCK8 assay was conducted to assess the proliferation of GES-1 cells following co-culture with TGES-1 cells. (C) The cloning efficiency of GES-1 cells was assessed following co-culture with TGES-1 cells. (D) The capabilities for migration and invasion were analyzed after co-culture. (E) Western blot analysis was performed to investigate the protein expression of EMT and stemness markers in GES-1 cells after co-culture with TGES-1 cells. (F) The mRNA expressions of genes associated with EMT and stemness characteristics in GES-1 cells were analyzed after co-culture. (G) The morphological characteristics of exosomes was characterized using TEM, scale bar: 100 nm. (H) The size of exosomes was detected by NTA. (I) The surface marker proteins of exosomes were detected by western blotting. (J) DAPI blue fluorescence labeled the nucleus and DiI red fluorescence labeled the exosomes. The uptake of extracellular vesicles by GES-1 cells was observed using confocal microscopy, original magnification, x60 (oil immersion). (K) The proliferation of cells was detected after treatment with exosomes derived from TGES-1 cells. (L) The cloning efficiency of cells was evaluated following treatment with TGES-1-EX. (M) The effect of exosomes from TGES-1 cells on the migration and invasion abilities of GES-1 cells was investigated, scale bar: 200 μm. (N) Western blot analysis was conducted to determine the protein levels of EMT and stemness markers in GES-1 cells after treatment with TGES-1-EX. (O) The mRNA levels of EMT and stemness markers were assessed after treatment with TGES-1-EX using RT-qPCR. *P<0.05, **P<0.01, ***P<0.001, ****P<0.0001. EMT, epithelial-mesenchymal transition; TEM, transmission electron microscopy; NTA, nanoparticle tracking analysis; RT-qPCR, reverse transcription-quantitative PCR; DiI, 1,1'-dioctadecyl-3,3,3',3'-tetramethylindocarbocyanine perchlorate; EX, exosome; TGES-1-EX, exosome secreted by TGES-1 cells.

blot analysis confirmed the presence of exosomal marker proteins, including HSP70, TSG101 and Alix, in both TGES-1 cells and their derived exosomes (Fig. 2I). To evaluate exosome uptake, TGES-1-EX were labeled with the fluorescent dye DiI, while cell nuclei were counterstained with DAPI. After incubation of labeled exosomes with GES-1 cells for 24 h, fluorescence microscopy revealed that DiI-labeled exosomes were efficiently internalized by GES-1 cells (Fig. 2J).

GES-1 cells were subsequently treated with TGES-1-EX for 72 h. CCK-8 assays showed that TGES-1-EX evidently promoted GES-1 cell growth (Fig. 2K). Colony formation and Transwell migration and invasion assays further demonstrated that TGES-1-EX enhanced the proliferative, migratory and invasive abilities of GES-1 cells (Fig. 2L and M). In addition, RT-qPCR and western blot analyses revealed that TGES-1-EX induced EMT and enhanced stemness-related properties in GES-1 cells (Fig. 2N and O). Collectively, these results indicated that MNNG promoted gastric carcinogenesis and that exosomes play a critical role in mediating intercellular communication during this process.

CircRNA 0000549 is highly expressed in TGES-1 cells, exosomes and serum exosomes. To further explore the molecular mechanisms underlying MNNG-induced malignant transformation, circRNA expression profiles were analyzed using two GEO datasets (GSE89143 and GSE93541) (Fig. 3A). Among the differentially expressed circRNAs, hsa_circ_0000549 (circ0000549, circSRSF5) was identified as notably upregulated in both GC tissues and plasma samples and has not been previously characterized (Fig. 3B). A heatmap showing the expression patterns of the shared circRNAs in tissue samples is provided in Fig. S1. According to circBase annotations (http://www.circbase.org/), circ0000549 is derived from the SRSF5 gene and is located at chr14:70236227-70236759, generated by circularization of exon 6 on human chromosome 14. Sanger sequencing confirmed that the amplified product was fully consistent with the predicted back-splice junction sequence (Fig. 3C). Agarose gel electrophoresis demonstrated that the RT-qPCR product of circ0000549 appeared as a single band with the expected size and showed no amplification from genomic DNA (gDNA), indicating that the primers specifically amplified circ0000549 from cDNA (Fig. 3D). Furthermore, RNase R digestion assays revealed that circ0000549 exhibited strong resistance to RNase R, confirming its circular structure and enhanced stability compared with its linear counterpart (Fig. 3E). Following treatment of TGES-1 cells with actinomycin D to inhibit transcription, the half-life of linear SRSF5 mRNA was ~4 h, whereas circ0000549 remained stable with a half-life of ~22 h (Fig. 3F). FISH analysis demonstrated that circ0000549 was distributed in both the nucleus and cytoplasm of TGES-1 cells (Fig. 3H). Collectively, these results indicate that circ0000549 is a highly stable circular RNA localized in both cellular compartments.

To confirm the expression of circ0000549 in TGES-1 cells, total RNA was extracted and analyzed by RT-qPCR, which confirmed that circ0000549 expression was notably elevated in TGES-1 cells. To determine whether MNNG-induced exosomes mediate the transfer of circ0000549 during gastric carcinogenesis, total RNA was isolated from exosomes derived from GES-1 and TGES-1 cells and circ0000549 expression was assessed by RT-qPCR. Circ0000549 was highly enriched in TGES-1 cells and their derived exosomes. Moreover, treatment of GES-1 cells with TGES-1-derived exosomes for 72 h resulted in a marked increase in circ0000549 expression (Fig. 3G and I).

To further evaluate the clinical relevance of circ0000549 in nitrite-induced GC, patients with GC were stratified based on dietary habits and exposure history to N-nitroso compounds, including long-term consumption of pickled foods, processed meat products and high-salt diets. Serum levels of N-nitrosoproline were subsequently measured to identify patients with high nitrate exposure (Fig. 3J). Notably, circ0000549 expression was elevated in serum exosomes from patients with GC with a history of high nitrite exposure (Fig. 3K). Receiver operating characteristic (ROC) curve analysis was performed to assess the diagnostic value of serum exosomal circ0000549 (n=40). The area under the ROC curve (AUC) was 0.7816, with a sensitivity of 64.52% and a specificity of 88.65% (Fig. 3L). In addition, serum-derived exosomes from patients with GC facilitated EMT, proliferation and stemness-related properties in GES-1 cells (Fig. 3M-O).

Circ0000549 promotes cell malignant properties. To investigate the functional role of circ0000549 in GC progression, two specific siRNAs targeting circ0000549 were designed to reduce its expression. siRNA-1 and siRNA-2 both efficiently suppressed circ0000549 expression in TGES-1 cells (Fig. 4A). CCK-8 assays and colony formation assays demonstrated that circ0000549 knockdown notably inhibited cell proliferation (Fig. 4B and C). In addition, Transwell assays revealed that silencing circ0000549 markedly reduced the migratory and invasive abilities of TGES-1 cells (Fig. 4D). Consistent with these functional changes, western blotting and RT-qPCR analyses showed that circ0000549 downregulation resulted in decreased expression of mesenchymal markers, proliferation-related proteins and stemness-associated factors, including N-cadherin, Vimentin, PCNA, OCT4, SOX2, Lin28 and Nanog, while the epithelial marker E-cadherin was upregulated (Fig. 4E and F).

Next, TGES-1 cells were transfected with a lentiviral vector overexpressing circ0000549 (Fig. 4G). Successful overexpression was confirmed following puromycin selection (Fig. 4H). Functional assays demonstrated that circ0000549 overexpression notably enhanced cell proliferation, migration and invasion (Fig. 4I-K). Moreover, western blotting and RT-qPCR analyses revealed that circ0000549 upregulation increased the expression of N-cadherin, Vimentin, PCNA, OCT4, SOX2, Lin28 and Nanog, while suppressing E-cadherin expression (Fig. 4L and M).

Exosomal circ0000549 facilitates migration, invasion, proliferation, EMT and stemness of GES-1 cells. Previous studies have shown that exosomes serve as important mediators of intercellular communication and can transfer specific non-coding RNAs to recipient cells, thereby altering their biological properties (32,33). To further explore whether circ0000549 exerts its effects through exosome-mediated transfer, TGES-1 cells were transfected with lentiviral vectors to knock down circ0000549 expression (Fig. 5A). The efficiency of circ0000549 silencing was confirmed after puromycin screening (Fig. 5B). Exosomes

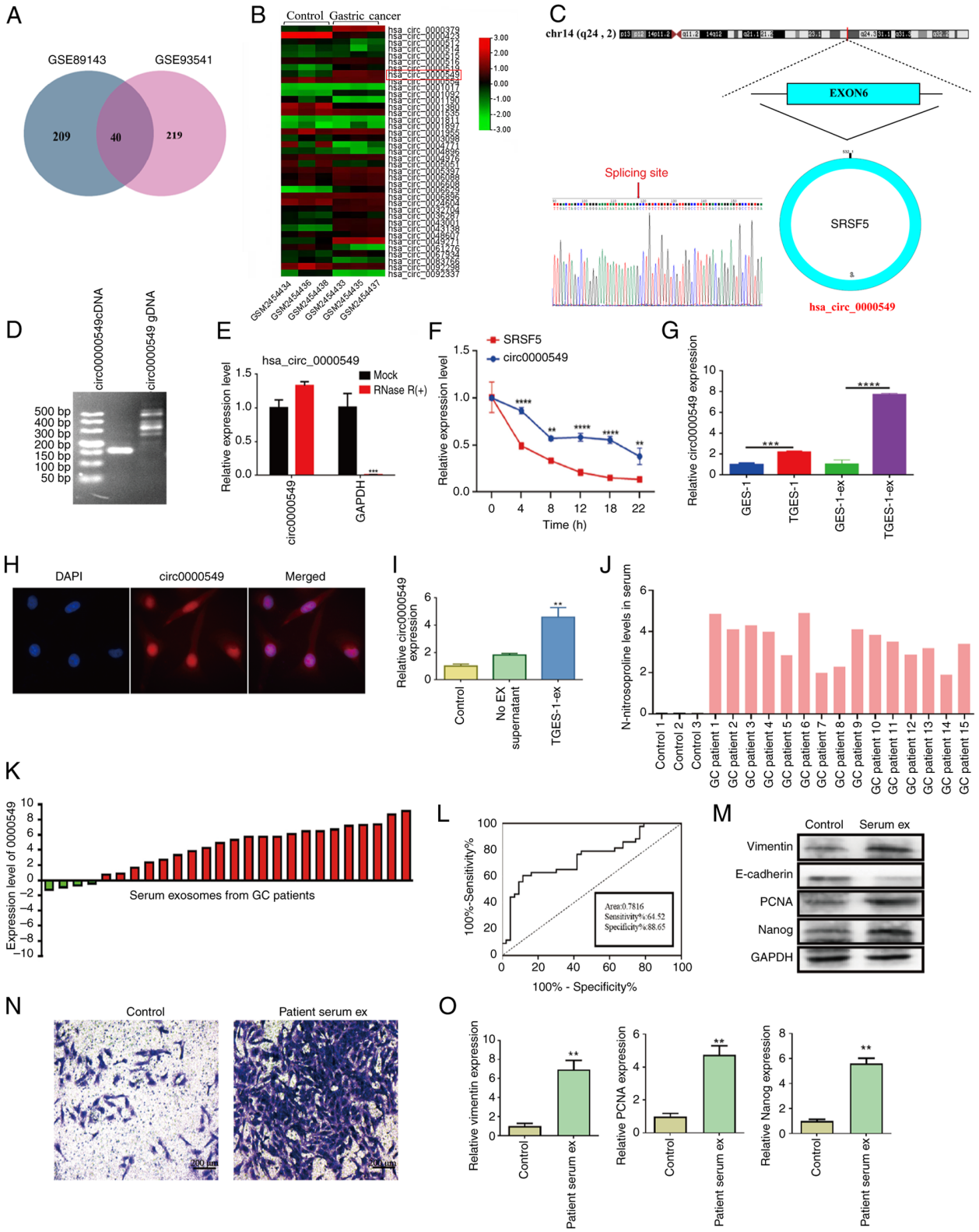

Figure 3. Characterization and expression of circ0000549 in TGES-1 cells and exosomes. (A) Coincidence was observed for the differentially expressed circular RNAs in the GEO database. (B) Heat map illustrating the differential expression of circRNAs, with circ0000549 standing out as highly expressed. (C) Diagram of the cyclization mechanism of circ0000549. (D) Verification through agarose gel electrophoresis showing the specificity of circ0000549 amplification from cDNA. (E) RT-qPCR results demonstrating the expression levels of circ0000549 before and after RNase R treatment, confirming its resistance to RNase R and stability compared to linear RNA. (F) The levels of circ0000549 and its parental gene SRSF5 were assessed after treatment with actinomycin D. (G) The expression of circ0000549 in TGES-1 cells and TGES-1-EX by RT-qPCR. (H) Localization of circ0000549 determined by FISH, original magnification, x60 (oil immersion). (I) The level of circ0000549 in GES-1 cells after TGES-1-EX treatment by RT-qPCR. (J) Serum levels of N-nitrosoproline were determined by LC-MS/MS. (K) The mRNA expression of circ0000549 in serum exosomes, n=26. (L) Diagnostic efficacy of serum exosome circ0000549, n=40. (M) Protein levels of EMT and stemness markers in GES-1 cells after treatment with serum exosomes. (N) The migration ability of GES-1 cells after treatment with serum exosomes, scale bar, 200 μm. (O) The mRNA expression of EMT and stemness markers in GES-1 cells after treatment with serum exosomes. **P<0.01, ***P<0.001, ****P<0.0001. GEO, Gene Expression Omnibus; RT-qPCR, reverse transcription-quantitative PCR; EMT, epithelial-mesenchymal transition; GC, gastric cancer; FISH, fluorescence *in situ* hybridization; Serum ex, serum derived exosomes from patients with gastric cancer; DAPI, 4',6-diamidino-2-phenylindole.

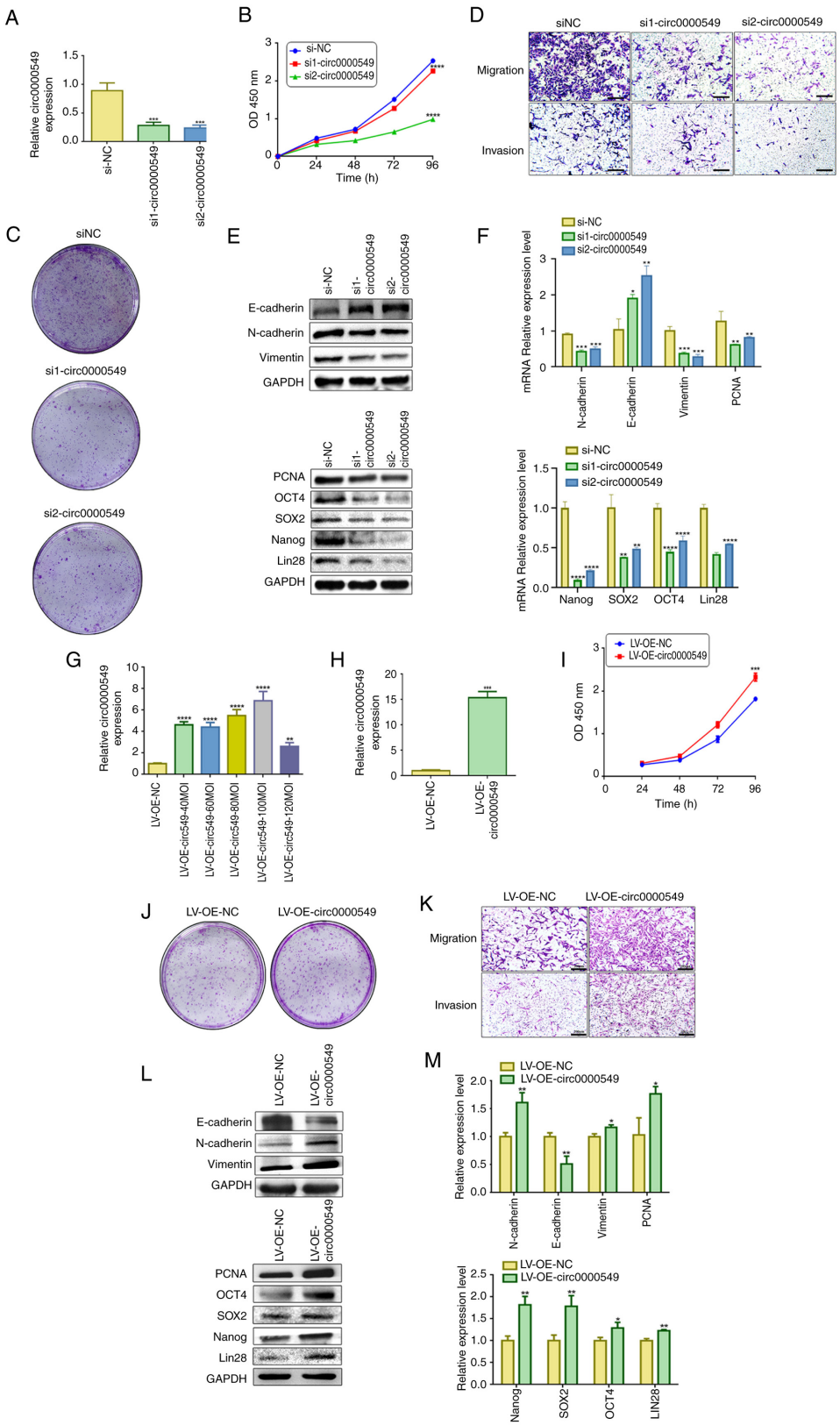

Figure 4. Circ0000549 promoted migration, proliferation, invasion and EMT in GES-1 cells. (A) The overexpression of circ0000549 in TGES-1 cells transfection with si1-circ0000549 and si2-circ0000549 was detected by RT-qPCR. (B) The effect of knocking down circ0000549 on the proliferation of TGES-1 cells was determined through a CCK-8 assay. (C) The effect of knocking down circ0000549 on the proliferative capacity of GES-1 cells was observed. (D) The abilities of TGES-1 cells to migrate and invade were evaluated, scale bar, 200 μm. (E) The protein levels of EMT-related and stemness were analyzed after knocking down circ0000549. (F) The mRNAs expression of EMT-related and stemness markers. (G) The level of circ0000549 in TGES-1 cells was measured 48 h post-transfection with a lentivirus designed to overexpress circ0000549. (H) The expression of circ0000549 after puromycin screening. (I) Assessed the proliferative capacity of TGES-1 cells following overexpression of circ0000549. (J) Changes in the clonogenic ability of TGES-1 cells after overexpression of circ0000549. (K) The effect of overexpression of circ0000549 on the migration and invasion abilities in TGES-1 cells, scale bar, 200 μm. (L) Changes in the levels of EMT-related and stemness protein after overexpression of circ0000549. (M) The expression of EMT-related and stemness mRNA in TGES-1 cells after overexpression of circ0000549. *P<0.05, **P<0.01, ***P<0.001, ****P<0.0001. EMT, epithelial-mesenchymal transition; RT-qPCR, reverse transcription-quantitative PCR; si1, siRNA1; si2, siRNA2; siNC, siRNA negative control; LV-OE-NC, lentivirus overexpression negative control; LV-OE, lentivirus overexpression; MOI, multiplicity of infection.

isolated from circ0000549 knockdown and overexpression cells were subsequently characterized (Fig. 5C-E). Total RNA was extracted from these exosomes and RT-qPCR analysis showed that circ0000549 levels in exosomes derived from circ0000549-knockdown cells were reduced by ~0.8-fold compared with control exosomes (sh-NC-EX). By contrast, exosomes derived from circ0000549-overexpressing cells exhibited an ~10-fold increase in circ0000549 expression relative to control exosomes (OE-NC-EX; Fig. 5F). GES-1 cells were then treated with exosomes containing either reduced or elevated circ0000549 levels. Functional assays demonstrated that exosomes derived from circ0000549-knockdown cells notably inhibited GES-1 cell migration, invasion, proliferation and stemness (Fig. 5H-J). Consistently, RT-qPCR and western blot analyses showed decreased expression of N-cadherin, Vimentin, PCNA, OCT4, SOX2, Lin28 and Nanog, accompanied by increased E-cadherin expression (Fig. 5J and K). By contrast, exosomes enriched with circ0000549 exerted the opposite effects on GES-1 cells (Fig. 5K and L). Collectively, these findings indicated that exosomal circ0000549 plays a critical role in promoting the malignant transformation of normal gastric epithelial cells.

miR-15b-5p serves as the target of circ0000549 and attenuates its protumorigenic effects. To further elucidate the molecular mechanism underlying circ0000549 function, the present study investigated its potential role as a competing endogenous RNA. CircRNAs are known to act as miRNA sponges in the cytoplasm and FISH analysis demonstrated that circ0000549 was distributed in both the nucleus and cytoplasm. In addition, CircInteractome analysis (https://circinteractome.nia.nih.gov/) predicted that circ0000549 could bind to AGO2, suggesting its involvement in miRNA-mediated regulation (Fig. 6A). It was therefore hypothesized that circ0000549 may function as a ceRNA to modulate MNNG-induced malignant phenotypes in GES-1 cells. Potential miRNAs interacting with circ0000549 were predicted using the StarBase, circBank and circAtlas databases. A total of six candidate miRNAs (miR-15b-5p, miR-16-5p, miR-545-3p, miR-145-5p, miR-1307-5p and miR-330-5p) were identified by overlapping predictions (Fig. 6B). Among these candidates, only miR-15b-5p was notably upregulated following circ0000549 knockdown, while circ0000549 overexpression resulted in a marked decrease in miR-15b-5p expression (Fig. 6C and D). In addition, miR-15b-5p was highly expressed in TGES-1 cells (Fig. 6E). To validate the direct interaction between circ0000549 and miR-15b-5p, circ0000549-WT and circ0000549-MUT binding sequences were cloned into dual-luciferase reporter plasmids. Co-transfection of circ0000549-WT with miR-15b-5p mimics notably reduced luciferase activity, whereas no significant change was observed in cells transfected with circ0000549-MUT or miR-NC (Fig. 6F). These results confirm that miR-15b-5p directly binds to circ0000549.

RT-qPCR analysis verified the transfection efficiency of miR-15b-5p mimics and inhibitors (Fig. 6G). Notably, circ0000549 expression was reduced following miR-15b-5p mimic transfection, while inhibition of miR-15b-5p increased circ0000549 levels, indicating a reciprocal regulatory relationship (Fig. 6H). Functionally, the promotive effects of circ0000549 overexpression on cell proliferation, migration and invasion were distinctly attenuated by miR-15b-5p mimics (Fig. 6I and K). Conversely, miR-15b-5p inhibition reversed the suppressive effects induced by circ0000549 knockdown, restoring the malignant phenotypes of GES-1 cells (Fig. 6I and K). Consistently, miR-15b-5p expression was reduced in GES-1 cells treated with circ0000549-overexpressing exosomes, whereas circ0000549-depleted exosomes produced the opposite effect (Fig. 6L). Collectively, these results indicate that circ0000549 promotes malignant transformation of GES-1 cells by sponging miR-15b-5p.

KIF1B is validated as a target gene of miR-15b-5p. Candidate target genes of miR-15b-5p were identified through intersection analysis of multiple online prediction databases, yielding six potential targets (Fig. 7A). Among these candidates, KIF1B was selected based on expression changes following circ0000549 and miR-15b-5p overexpression or knockdown (Fig. 7B). RT-qPCR analysis confirmed that KIF1B expression was distinctly elevated in TGES-1 cells (Fig. 7C). A previous study has reported that KIF1B functions as a downstream effector of oncogenic circRNAs, such as CircPOSTN in glioma (34). Consistent with this, co-transfection of circ0000549 overexpression plasmids and miR-15b-5p mimics distinctly reduced KIF1B expression, whereas co-transfection of circ0000549 siRNA and miR-15b-5p inhibitors markedly increased KIF1B levels (Fig. 7D). Dual-luciferase reporter assays further demonstrated that miR-15b-5p overexpression markedly decreased luciferase activity in cells transfected with WT KIF1B constructs, while no significant effect was observed in MUT constructs (Fig. 7E).

Exosomal circ0000549 facilitates malignant progression through the miR-15b-5p/KIF1B/PI3K/AKT signaling pathway. GeneCards database analysis predicted that KIF1B is functionally associated with the PI3K/AKT signaling pathway (Fig. 7F). Western blot analysis showed that circ0000549 overexpression activated the PI3K/AKT pathway, whereas circ0000549 knockdown suppressed pathway activation (Fig. 7G). Similarly, exosomes enriched with circ0000549 increased the levels of phosphorylated PI3K and AKT in GES-1 cells, while circ0000549-depleted exosomes exerted the opposite effects (Fig. 7H). To further verify the involvement of KIF1B, siRNA targeting KIF1B was transfected into TGES-1 cells (Fig. 7I). Overexpression of circ0000549-containing exosomes partially rescued the reduction in KIF1B expression caused by KIF1B knockdown (Fig. 7J). Western blot analysis further revealed that KIF1B silencing inhibited PI3K/AKT signaling, whereas circ0000549-overexpressing exosomes restored PI3K and p-AKT expression (Fig. 7K). Functionally, KIF1B knockdown remarkably suppressed cell migration, invasion and proliferation, while circ0000549-enriched exosomes alleviated these inhibitory effects (Fig. 7L and N). These findings suggested that exosomal circ0000549 promotes malignant transformation of GES-1 cells through the miR-15b-5p/KIF1B/PI3K/AKT signaling axis.

Exosomal circ0000549 enhances tumorigenicity, EMT, proliferation and stem-like properties in vivo. As GES-1 cells lack intrinsic tumorigenicity, TGES-1 cells were used for *in vivo* validation. Exosomes with circ0000549 knockdown

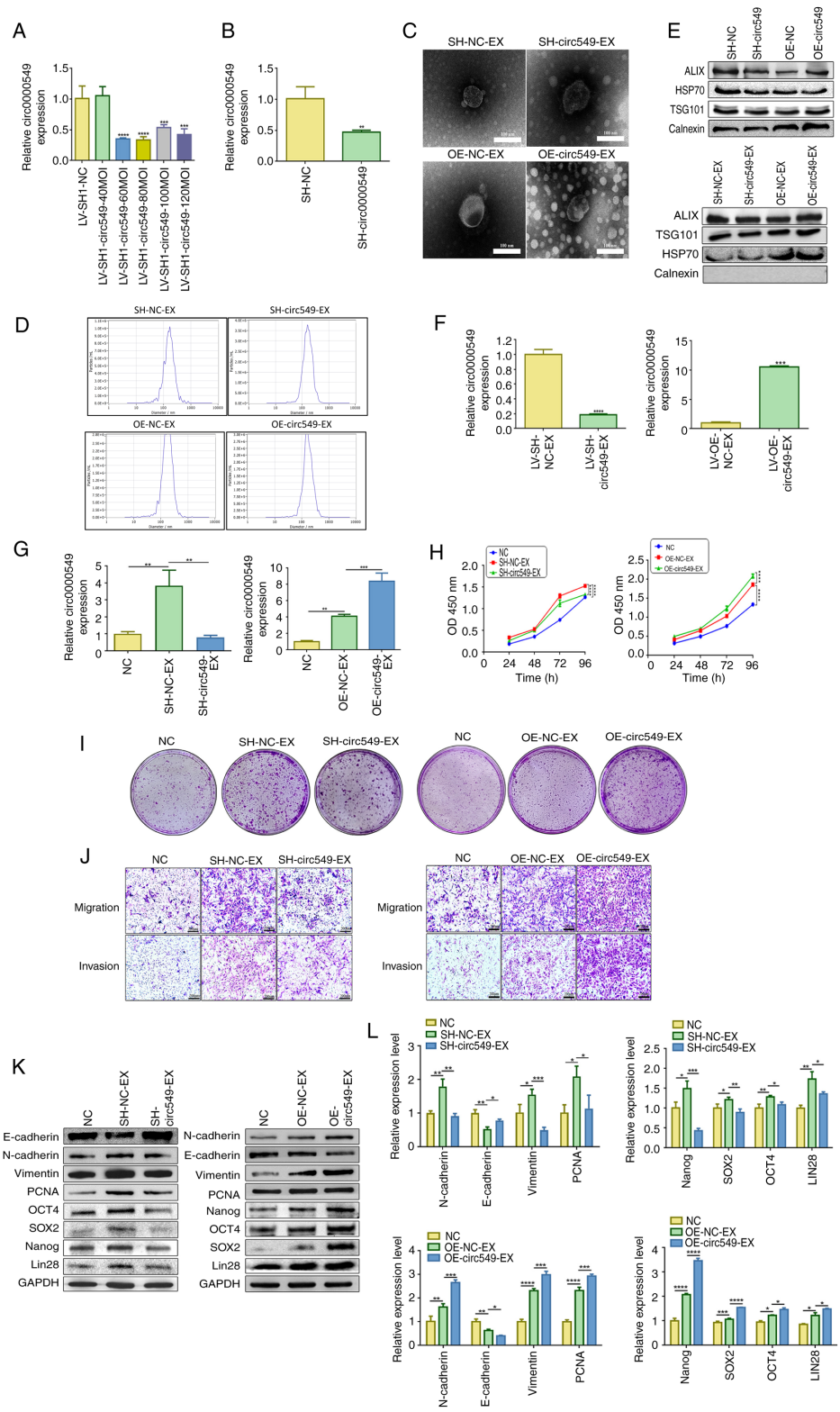

Figure 5. Exosomal circ0000549 promotes the proliferation, migration, invasion, EMT and stemness in GES-1 cells. (A) Measure the level of circ0000549 in TGES-1 cells 48 h post-transfection with a lentivirus designed for circ0000549 knockdown. (B) The level of circ0000549 after puromycin screening. (C) The knockdown/overexpression of exosomes was detected by TEM, scale bar, 100 nm. (D) The size of exosomes was determined using NTA. (E) The protein levels of surface markers of exosomes were detected. (F) The levels of circ0000549 in TGES-1-EX with knockdown/overexpression of circ0000549. (G) The level of circ0000549 in GES-1 cells after SH-circ0000549-EX/OE-circ0000549-EX treatment. (H) Assessment of GES-1 cell proliferation post-treatment with SH-circ0000549-EX/OE-circ0000549-EX. (I) Evaluation of the clonality of GES-1 cells after SH-circ0000549-EX/OE-circ0000549-EX treatment. (J) Examination of the migratory and invasive capabilities of GES-1 cells following SH-circ0000549-EX/OE-circ0000549-EX treatment, scale bar, 200 μm. (K) Determination of EMT and stemness protein expression levels in GES-1 cells treated SH-circ0000549-EX/OE-circ0000549-EX. (L) Quantification of EMT and stemness mRNA levels in GES-1 cells after SH-circ0000549-EX/OE-circ0000549-EX treatment using RT-qPCR. *P<0.05, **P<0.01, ***P<0.001, ****P<0.0001. TEM, transmission electron microscopy; NTA, nanoparticle tracking analysis; RT-qPCR, reverse transcription-quantitative PCR; NC, negative control; EX, exosome; OE-circ549-EX, exosomes from TGES-1 cells treated with circ0000549 lentivirus overexpression; OE-NC-EX, exosomes from TGES-1 cells treated with circ0000549 lentivirus overexpression negative control; SH-circ0000549-EX, exosomes from TGES-1 cells treated with circ0000549 lentivirus knockdown; SH-NC-EX; exosomes from TGES-1 cells treated with circ0000549 lentivirus knockdown negative control; MOI, multiplicity of infection.

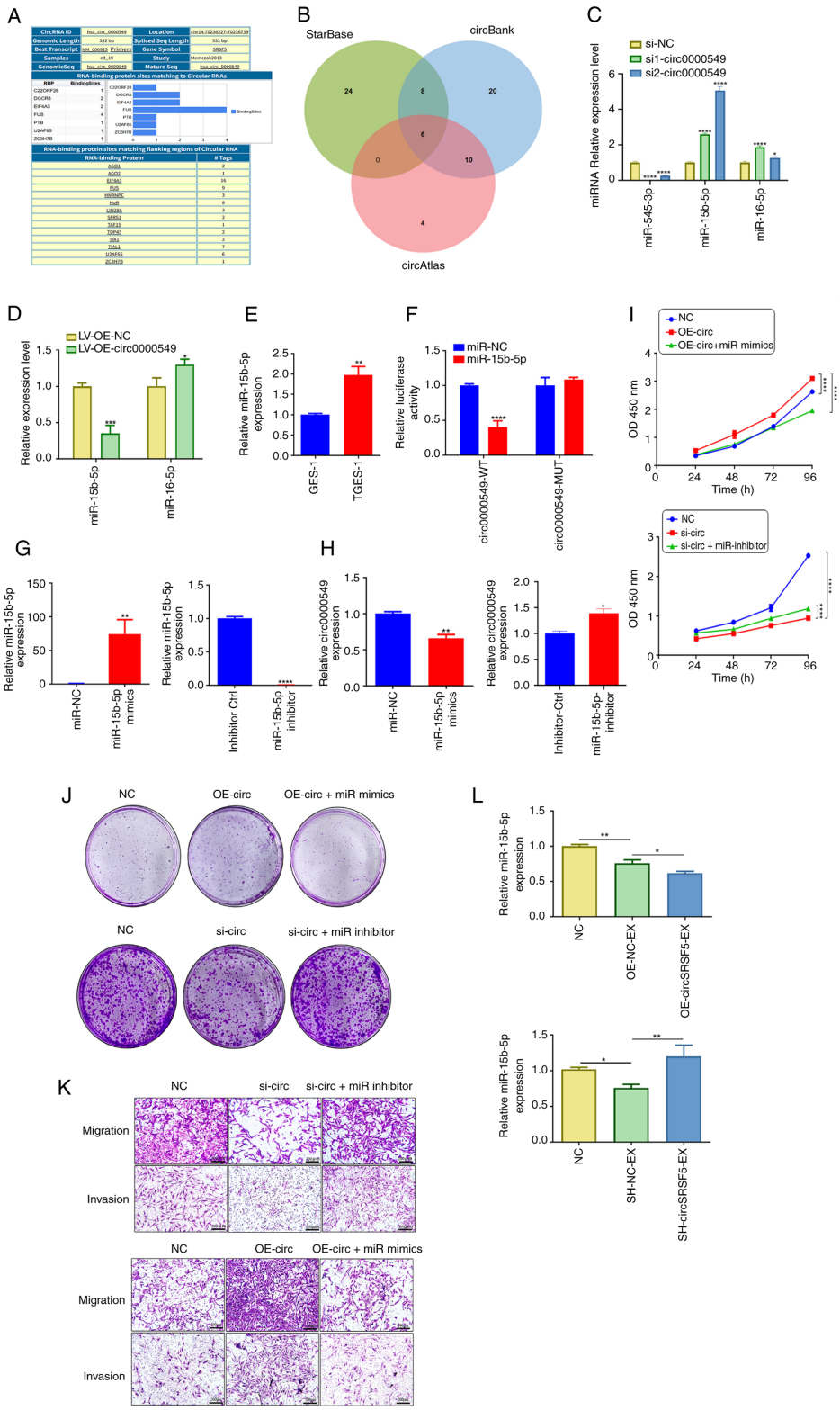

Figure 6. miR-15b-5p is the target of circ0000549 and weakens the protumor effect of circ0000549. (A) circInteractome database showed that AGO2 had binding ability with the flanking region of circ0000549. (B) The online database predicted the intersection of miRNA bound by circ0000549. (C) The expression of miRNA after knocking down circ0000549 by RT-qPCR. (D) The level of miRNA after overexpression of circ0000549 by RT-qPCR. (E) The expression of miR-15b-5p was assessed. (F) A dual luciferase reporter gene assay was conducted to investigate the interaction between circ0000549 and miR-15b-5p. (G) The level of miR-15b-5p expression in TGES-1 cells was assessed following transfection with miR-15b-5p mimics or an inhibitor. (H) The level of circ0000549 was assessed following transfection with miR-15b-5p mimics or an inhibitor. (I) The proliferation of cells was evaluated after co-transfecting them with OE-circ0000549 and miR-15b-5p mimics, or with si-circ0000549 and miR-15b-5p inhibitor. (J) Evaluation of the clonality of TGES-1 cells after co-transfection of OE-circ0000549 and miR-15b-5p mimics/ si-circ0000549 and miR-15b-5p inhibitor. (K) The migration and invasion capabilities of TGES-1 cells were assessed following co-transfection with OE-circ0000549 and miR-15b-5p mimics, or with si-circ0000549 and miR-15b-5p inhibitor, scale bar, 200 μm. (L) Level of miR-15b-5p following SH-circ0000549-EX/OE-circ0000549-EX treatment by RT-qPCR. *P<0.05, **P<0.01, ***P<0.001, ****P<0.0001. RT-qPCR, reverse transcription-quantitative PCR; si1, siRNA1; si2, siRNA2; siNC, siRNA negative control; LV-OE-NC, lentivirus overexpression negative control; LV-OE, lentivirus overexpression; WT, Wild Type; MUT, Mutant; miR-NC, miR-15b-5p mimics negative control; inhibitor Ctrl, miR-15b-5p inhibitor control; OE-circ, lentivirus overexpression of circ0000549; miR mimics, miR-15b-5p mimics; miR-inhibitor, miR-15b-5p inhibitor.

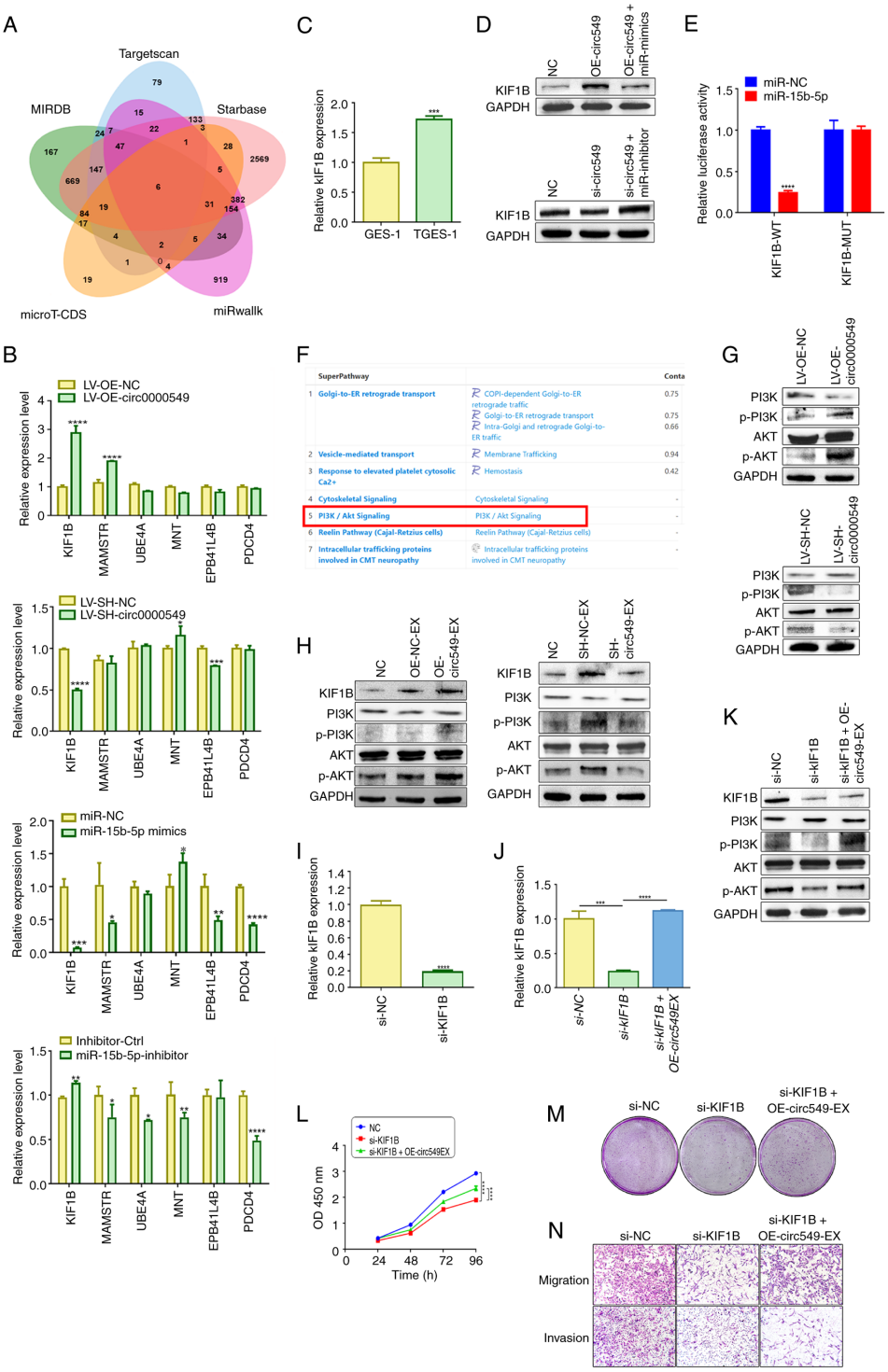

Figure 7. Circ0000549 in exosomes aids in promoting the aggressive evolution of GES-1 cells, mainly through miR-15b-5p/KIF1B/PI3K/AKT axis. (A) Internet databases were used to predict which genes are regulated by miR-15b-5p. (B) The levels of candidate target genes after knockdown/overexpression of circ0000549 or transfection of miR-15b-5p mimics/inhibitor by RT-qPCR. (C) mRNA level of KIF1B was detected. (D) The effect of co transfection with OE circ0000549 and miR-15b-5p mimic/si circ00000549 and miR-15b-5p inhibitor on the expression of KIF1B. (E) A dual luciferase reporter gene assay was employed to elucidate the interaction between KIF1B and miR-15b-5p. (F) GeneCards database was used to predict KIF1B downstream pathways online. (G) The pathway activity of the PI3K/AKT in TGES-1 cells after knocking down/overexpressing circ0000549. (H) Changes in expression levels of KIF1B and PI3K/AKT pathway proteins of GES-1 cells after SH-circ0000549-EX/OE-circ0000549-EX treatment. (I) The effect on KIF1B level in TGES-1 cells subsequent to KIF1B knockdown. (J) The level of KIF1B in TGES-1 cells which was knocked down KIF1B after treatment with OE-circ0000549 exosomes by RT-qPCR. (K) Detection of changes in expression levels of KIF1B and PI3K/AKT pathway proteins in TGES-1 cells which was knocked down KIF1B after treatment with OE-circ0000549 exosomes. (L) Detection of changes in the proliferation ability of TGES-1 cells. (M) Clonality of TGES-1 cells which was knocked down KIF1B after treatment with OE-circ0000549 exosomes. (N) Alterations in the migratory and invasive capabilities of TGES-1 cells treated with OE-circ0000549 exosomes and KIF1B knockdown in combination. *P<0.05, **P<0.01, ***P<0.001, ****P<0.0001. miR, microRNA; RT-qPCR, reverse transcription-quantitative PCR; NC, negative control; LV-OE-NC, lentivirus overexpression negative control; LV-OE, lentivirus overexpression; LV-SH-circ0000549, lentivirus knockdown of circ0000549; LV-SH-NC; lentivirus knockdown of circ0000549 negative control; miR-NC, miR-15b-5p mimics negative control; inhibitor Ctrl, miR-15b-5p inhibitor control; OE-circ549, lentivirus overexpression of circ0000549; OE-circ549-EX, exosomes from TGES-1 cells treated with circ0000549 lentivirus overexpression; siKIF1B, siRNA of KIF1B; siNC, siRNA negative control; SH-circ549-EX, exosomes from TGES-1 cells treated with circ0000549 lentivirus knockdown; SH-NC-EX; exosomes from TGES-1 cells treated with circ0000549 lentivirus knockdown negative control.

evidently reduced tumor formation rate, tumor size and tumor volume in nude mice (Fig. 8A-C). Analysis of tumor tissues revealed that circ0000549 expression was markedly decreased in the circ0000549 knockdown exosome group (Fig. 8D). Furthermore, western blotting and RT-qPCR analyses showed reduced expression of Vimentin, PCNA and Nanog, accompanied by increased E-cadherin expression (Fig. 8E and F). Immunohistochemical staining yielded consistent results (Fig. 8G), indicating that circ0000549 regulates EMT, proliferation and stemness *in vivo*.

miR-15b-5p mediates circ0000549-driven TGES-1 tumorigenesis in vivo. To further validate the circ0000549/miR-15b-5p axis *in vivo*, nude mice were divided into three groups: TGES-1, TGES-1 treated with circ0000549-overexpressing exosomes and TGES-1 treated with circ0000549-overexpressing exosomes combined with miR-15b-5p mimics. Overexpression of circ0000549 evidently enhanced the tumorigenicity of TGES-1 cells, whereas co-treatment with miR-15b-5p mimics markedly attenuated this effect (Fig. 8H and I). Moreover, combined treatment resulted in decreased expression of Vimentin, PCNA and Nanog, along with increased E-cadherin expression, as confirmed by western blotting, RT-qPCR and immunohistochemical analyses (Fig. 8J and L). These results demonstrate that circ0000549 promotes tumorigenicity, EMT, proliferation and stemness of TGES-1 cells in a miR-15b-5p-dependent manner.

Discussion

GC is one of the most prevalent malignant tumors worldwide (35). Early GC is often asymptomatic and is therefore frequently diagnosed at advanced stages. The incidence of GC shows marked geographic variation, which may be closely associated with genetic background, lifestyle and environmental factors, particularly dietary habits. Among these factors, dietary nitrite intake has been recognized as one of the most important contributors to gastric carcinogenesis (36). MNNG has been shown to induce precancerous lesions, malignant transformation and tumor formation in animal models (37). As a representative nitroso compound, MNNG is widely used to simulate nitrosamine-induced gastric mucosal carcinogenesis both *in vivo* and *in vitro* (38). The present study demonstrated that long-term exposure to MNNG is sufficient to induce malignant transformation of human gastric epithelial cells. However, despite extensive evidence supporting its carcinogenic potential, the precise molecular mechanisms by which MNNG promotes GC initiation and progression remain incompletely understood.

Within the TME, tumor cell-derived exosomes function as important mediators of intercellular communication, facilitating information exchange between malignant cells and neighboring normal cells and thereby promoting tumor growth, invasion and metastasis (39). Exosomes are nanoscale extracellular vesicles with diameters ranging from 30-200 nm, capable of selectively encapsulating a variety of bioactive molecules from donor cells, including lipids, proteins, non-coding RNAs, nucleic acids and metabolites (24,40). An increasing body of evidence has demonstrated that circRNAs are involved in the initiation and progression of numerous diseases and exert critical regulatory roles in diverse physiological and pathological processes (41-44). In particular, exosome-mediated transfer of circRNAs is critical in tumor development and progression, including GC. For instance, Zheng *et al* (45) reported that exosome-transmitted circATG4B contributes to reduced chemosensitivity in colorectal cancer cells, highlighting a potential therapeutic strategy to overcome oxaliplatin resistance. Similarly, Lin *et al* (46) demonstrated that hypoxia-induced exosomes carrying circPDK1 enhance glycolysis in pancreatic cancer cells by modulating the miR-628-3p/BPTF axis and promoting BIN1 degradation, thereby elevating c-Myc expression. Despite these advances, the roles and molecular mechanisms of circRNAs in the malignant transformation of normal cells induced by environmental carcinogens remain poorly understood.

In the present study, normal GES-1 cells were treated with MNNG-induced exosomes and it was observed that these exosomes promoted malignant transformation of GES-1 cells in a manner comparable to direct MNNG exposure. Analysis of GEO datasets (GSE89143 and GSE93541) revealed that circ0000549 was highly expressed in GC tissues, malignantly transformed GES-1 cells and their derived exosomes, leading us to select circ0000549 as the focus of this investigation. We further demonstrated that circ0000549 carried by TGES-1-derived exosomes was capable of inducing malignant transformation of GES-1 cells. To elucidate the functional role and molecular mechanism of circ0000549 in GC progression, the present study performed a series of experimental analyses guided by bioinformatic predictions. The results showed that circ0000549 promotes KIF1B expression through competitive binding to miR-15b-5p. KIF1B has previously been reported to regulate tumor progression in glioma and hepatocellular carcinoma (34,47). Bioinformatic analysis further suggested that KIF1B is functionally associated with the PI3K/AKT signaling pathway. Consistent with these predictions, the findings of the present study indicated that the MNNG-induced exosomal circ0000549/miR-15b-5p/KIF1B axis regulates the proliferative, migratory and invasive capacities of normal gastric epithelial cells by activating the PI3K/AKT pathway and promoting the EMT process, thereby facilitating malignant transformation and the initiation of GC.

Taken together, the findings demonstrate that exosomal circ0000549 promotes the malignant progression of surrounding normal gastric epithelial cells through the miR-15b-5p/KIF1B/PI3K/AKT signaling axis. These results suggested that the exosomal circ0000549/miR-15b-5p/KIF1B axis may represent a promising therapeutic target for the prevention and treatment of nitrite-induced GC. Moreover, the present study provided important mechanistic evidence supporting the clinical management of gastric precancerous lesions and the potential delay of GC progression. Although the present study focused on circ0000549, it does not exclude the possibility that other exosomal components derived from MNNG-transformed cells, such as oncogenic microRNAs or proteins, may also contribute to the priming of recipient cells. Nevertheless, the circ0000549 knockdown and rescue experiments indicate that circ0000549 accounts for a substantial proportion of the observed effects, underscoring its predominant role among the oncogenic cargos carried by exosomes.

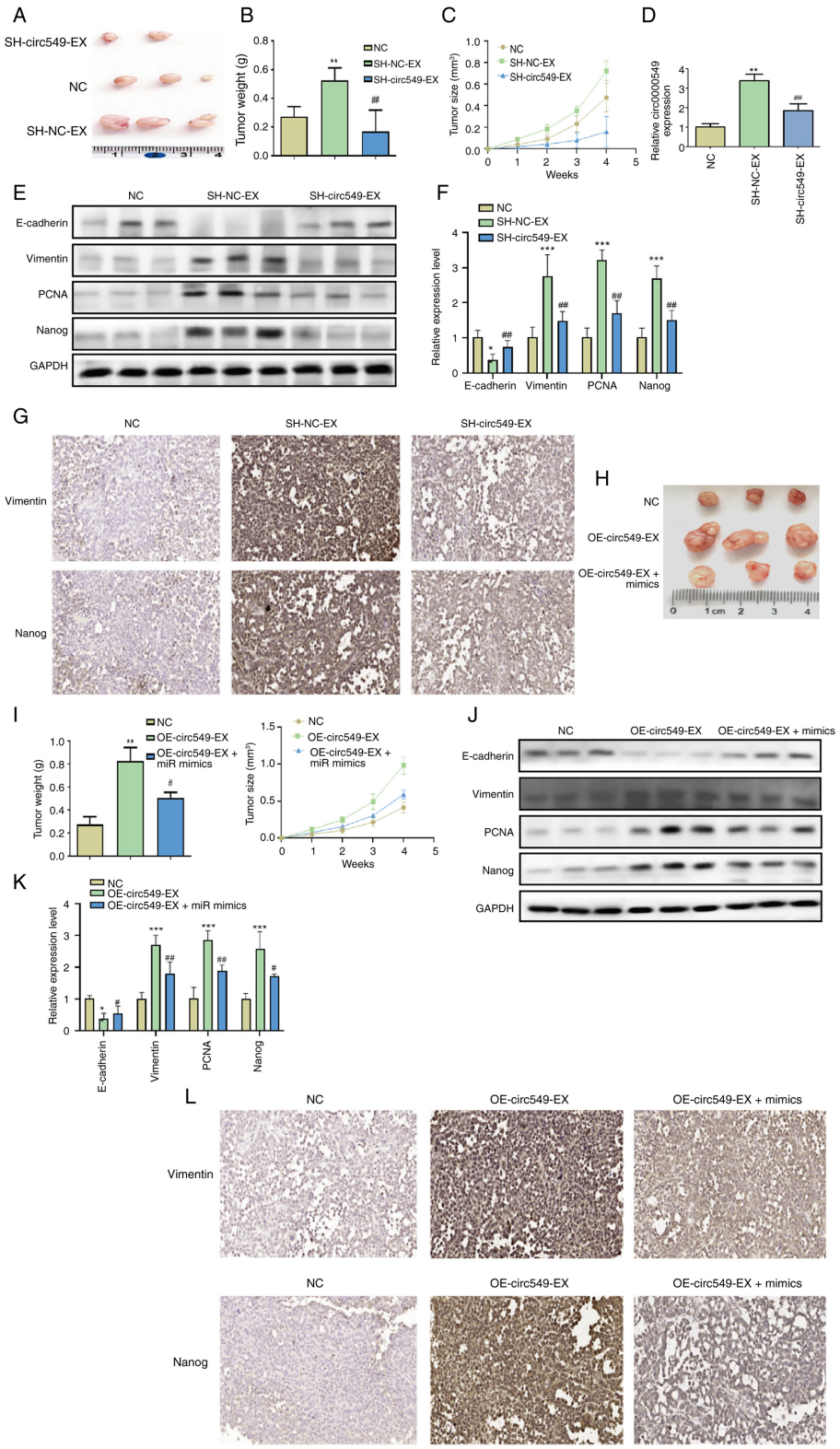

Figure 8. Exosomal circ0000549 tumorigenicity, EMT, proliferation and stemness. (A) The downregulation of circ0000549 impairs the tumorigenic capacity of TGES-1 cells. (B) The effect of SH-circ0000549-EX treatment on tumor weight. (C) The effect of SH-circ0000549-EX treatment on tumor volume. (D) The level of circ0000549 in tumor tissues after SH-circ0000549-EX treatment by RT-qPCR. (E) The levels of stemness, EMT and proliferation proteins in tumor tissues after SH-circ0000549-EX treatment. (F) The mRNA expression of stemness, EMT and proliferation makers mRNA in tumor tissues after SH-circ0000549-EX treatment. (G) Immunohistochemical analysis of tumor tissues treated with SH-circ0000549-EX revealed alterations in the levels of EMT and stemness markers, magnification, x400. (H) The effect of OE-circ0000549-EX alone or in combination with miR-15b-5p mimic on the tumorigenicity of TGES-1 cells. (I) The effect of OE-circ0000549-EX alone or in combination with miR-15b-5p mimic on tumor weight and volume. (J) The levels of stemness, EMT and proliferation-related markers in tumor tissues following treatment with OE-circ0000549-EX alone or in combination with miR-15b-5p mimic. (K) The expression of stemness, EMT and proliferation mRNA in tumor tissues after treated with OE-circ0000549-EX alone or in combination with miR-15b-5p mimic. (L) The levels of vimentin and Nanog in tumor tissues after SH-circ0000549-EX treatment by Immunohistochemistry, magnification, x200. *P<0.05, **P<0.01, ***P<0.001, $^{\#}$P<0.05, $^{\#\#}$P<0.01. EMT, epithelial-mesenchymal transition; RT-qPCR, reverse transcription-quantitative PCR; NC, negative control; SH-circ549-EX, exosomes from TGES-1 cells treated with circ0000549 lentivirus knockdown; SH-NC-EX; exosomes from TGES-1 cells treated with circ0000549 lentivirus knockdown negative control; OE-circ549-EX, exosomes from TGES-1 cells treated with circ0000549 lentivirus overexpression.

In conclusion, the present study demonstrated that long-term exposure to MNNG induces malignant transformation of GES-1 cells, with exosomes playing a pivotal role in mediating intercellular communication during this process. Specifically, exosomal circ0000549 was identified as a key driver of gastric carcinogenesis by activating the PI3K/AKT signaling pathway and promoting malignant transformation of normal gastric epithelial cells through the miR-15b-5p/KIF1B axis. These findings revealed a previously unrecognized regulatory mechanism involving exosomal circRNAs in MNNG-induced GC development.

Acknowledgements

Not applicable.

Funding

The present study was generously supported by funding from the National Natural Science Foundation of China (grant no. 81602883), Technology Development Project of Jiangsu University (grant nos. 20220014 and 20220516) and Postgraduate Research and Practice Innovation Program of Jiangsu Province (grant no. KYCX25_ 4287).

Availability of data and materials

The data generated in the present study may be requested from the corresponding author. The data of LC-MS/MS have been submitted to the OMIX repository of the National Genomics Data Center under accession number OMIX014373-02 (BioProject: PRJCA055549) and are publicly accessible at: https://ngdc.cncb.ac.cn/omix/preview/tVgV3viP or https://ngdc.cncb.ac.cn/gsub/submit/bioproject/PRJCA055549.

Authors' contributions

ZL was responsible for conceptualization, methodology, software, resources, data analysis, writing the original draft and manuscript revision. ZG and YZ were responsible for data curation, data analysis, methodology and writing the original draft. JS was responsible for data analysis and investigation. HQ was responsible for writing, reviewing and editing and supervision. XX was responsible for writing, reviewing and editing, conceptualization, methodology and resources. ZL and YZ confirm the authenticity of all the raw data. All authors read and approved the final manuscript.

Ethics approval and consent to participate

All mouse experiments conducted in the present study were approved by the Animal Care and Use Committee of Jiangsu University (approval no. UJS-IACUC-AP-2023030801). Every effort was made to minimize animal suffering and distress throughout the experimental procedures. The collection of human samples in the present study was approved by the Medical Ethics Committee of Jiangsu University (ethics approval no. 2023182). Written informed consent was obtained from each participant, who also agreed to the use of the relevant experimental data for publication.

Patient consent for publication

Not applicable.

Competing interests

The authors declare that they have no competing interests.

References

1. Siegel RL, Kratzer TB, Giaquinto AN, Sung H and Jemal A: Cancer statistics, 2025. CA Cancer J Clin 75: 10-45, 2025.
2. Diao X, Guo C, Jin Y, Li B, Gao X, Du X, Chen Z, Jo M, Zeng Y, Ding C, *et al*: Cancer situation in China: An analysis based on the global epidemiological data released in 2024. Cancer Commun (Lond) 45: 178-197, 2025.
3. Malik TH, Sayahan MY, Al Ahmed HA and Hong X: Gastric intestinal metaplasia: An intermediate precancerous lesion in the cascade of gastric carcinogenesis. J Coll Physicians Surg Pak 27: 166-172, 2017.
4. Wang Q, Huang Y, Jiang M, Tang Y, Wang Q, Bai L, Yu C, Yang X, Ding K, Wang W, *et al*: The demethylase ALKBH5 mediates ZKSCAN3 expression through the m^6A modification to activate VEGFA transcription and thus participates in MNNG-induced gastric cancer progression. J Hazard Mater 473: 134690, 2024.
5. Xia C, Dong X, Li H, Cao M, Sun D, He S, Yang F, Yan X, Zhang S, Li N and Chen W: Cancer statistics in China and United States, 2022: Profiles, trends, and determinants. Chin Med J (Engl) 135: 584-590, 2022.
6. Chiavarini M, Bertarelli G, Minelli L and Fabiani R: Dietary intake of meat cooking-related mutagens (HCAs) and risk of colorectal adenoma and cancer: A systematic review and meta-analysis. Nutrients 9: 514, 2017.
7. Wu X, Chen L, Cheng J, Qian J, Fang Z and Wu J: Effect of dietary salt intake on risk of gastric cancer: A systematic review and meta-analysis of case-control studies. Nutrients 14: 4260, 2022.
8. Schoental R: Carcinogenic activity of N-methyl-N-nitroso-N'-nitroguanidine. Nature 209: 726-727, 1966.
9. Liu T, Feng YL, Wang RY, Yang S, Ge YL, Zhang TY, Li J, Li CY, Ruan Y, Luo B and Liang GY: Long-term MNNG exposure promotes gastric carcinogenesis by activating METTL3/m6A/miR1184 axis-mediated epithelial-mesenchymal transition. Sci Total Environ 913: 169752, 2024.
10. Wsierska-Gadek J, Gueorguieva M and Wojciechowski J: MNNG induces dramatic DNA damage and non-apoptotic changes in cervical carcinoma HeLa cells. Ann NY Acad Sci 1010: 278-282, 2003.
11. Wang Y, Chu F, Lin J, Li Y, Johnson N, Zhang J, Gai C, Su Z, Cheng H, Wang L and Ding X: Erianin, the main active ingredient of Dendrobium chrysotoxum Lindl, inhibits precancerous lesions of gastric cancer (PLGC) through suppression of the HRAS-PI3K-AKT signaling pathway as revealed by network pharmacology and in vitro experimental verification. J Ethnopharmacol 279: 114399, 2021.
12. Zhao Y, Sun Y, Wang G, Ge S and Liu H: Dendrobium officinale polysaccharides protect against MNNG-induced PLGC in rats via activating the NRF2 and antioxidant enzymes HO-1 and NQO-1. Oxid Med Cell Longev 2019: 9310245, 2019.
13. Liang M, Liu Z, Lin H, Shi B, Li M, Chen T, Qin L, Niu Q, Yu G, Jiang H and Zhou X: High-throughput sequencing reveals circular RNA hsa_circ_0000592 as a novel player in the carcinogenesis of gastric carcinoma. Biosci Rep 39: BSR20181900, 2019.
14. Zhu F, Xu Y, Pan J, Li M, Chen F and Xie G: Epigallocatechin gallate protects against MNNG-induced precancerous lesions of gastric carcinoma in rats via PI3K/Akt/mTOR pathway. Evid Based Complement Alternat Med 2021: 8846813, 2021.
15. Xu J, Shen W, Pei B, Wang X, Sun D, Li Y, Xiu L, Liu X, Lu Y, Zhang X and Yue X: Xiao Tan He Wei Decoction reverses MNNG-induced precancerous lesions of gastric carcinoma in vivo and vitro: Regulation of apoptosis through NF-κB pathway. Biomed Pharmacother 108: 95-102, 2018.
16. Zhao Y, Li B, Wang G, Ge S, Lan X, Xu G and Liu H: Dendrobium officinale polysaccharides inhibit 1-methyl-2-nitro-1-nitrosoguanidine induced precancerous lesions of gastric cancer in rats through regulating Wnt/β-catenin pathway and altering serum endogenous metabolites. Molecules 24: 2660, 2019.

17. Zhang Y, Chen Z, Song J, Qian H, Wang Y and Liang Z: The role of m6A modified circ0049271 induced by MNNG in precancerous lesions of gastric cancer. Heliyon 10: e35654, 2024.
18. Liu W, Niu J, Huo Y, Zhang L, Han L, Zhang N and Yang M: Role of circular RNAs in cancer therapy resistance. Mol Cancer 24: 55, 2025.
19. Kristensen LS, Andersen MS, Stagsted LVW, Ebbesen KK, Hansen TB and Kjems J: The biogenesis, biology and characterization of circular RNAs. Nat Rev Genet 20: 675-691, 2019.
20. Conn VM, Chinnaiyan AM and Conn SJ: Circular RNA in cancer. Nat Rev Cancer 24: 597-613, 2024.
21. Lin Z, Zhong C, Shi M, Long Q, Jing L, Yu Y, Chou J, Chen M, Lan M and Long F: Circular RNA TFRC/SCD1 mRNA interaction regulates ferroptosis and metastasis in gastric cancer. Cell Death Dis 16: 436, 2025.
22. Zhou G, Wen J, Lu F, Wang J and Tan S: circRNA_0005927 inhibits gastric cancer metastasis by downregulating the miR-570-3p/FOXO3 axis. Am J Transl Res 17: 1679-1693, 2025.
23. Glaviano A, Lau HS, Carter LM, Lee EHC, Lam HY, Okina E, Tan DJJ, Tan W, Ang HL, Carbone D, *et al*: Harnessing the tumor microenvironment: Targeted cancer therapies through modulation of epithelial-mesenchymal transition. J Hematol Oncol 18: 6, 2025.
24. Li J, Wang A, Guo H, Zheng W, Chen R, Miao C, Zheng D, Peng J, Wang J and Chen Z: Exosomes: Innovative biomarkers leading the charge in non-invasive cancer diagnostics. Theranostics 15: 5277-5311, 2025.
25. Zheng Z, Zhai Y, Yan X, Wang Z, Zhang H, Xu R, Liu X, Cai J, Zhang Z, Shang Y, *et al*: Functions and clinical applications of exosomes in gastric cancer. Int J Biol Sci 21: 2330-2345, 2025.
26. Paskeh MDA, Entezari M, Mirzaei S, Zabolian A, Saleki H, Naghdi MJ, Sabet S, Khoshbakht MA, Hashemi M, Hushmandi K, *et al*: Emerging role of exosomes in cancer progression and tumor microenvironment remodeling. J Hematol Oncol 15: 83, 2022.
27. Yang R, Qu X, Zhi S, Wang J, Fu J, Tan C, Chen H and Wang X: Exosomes derived from meningitic escherichia coli-infected brain microvascular endothelial cells facilitate astrocyte activation. Mol Neurobiol 61: 7195-7210, 2024.
28. Huang XJ, Wang Y, Wang HT, Liang ZF, Ji C, Li XX, Zhang LL, Ji RB, Xu WR, Jin JH and Qian H: Exosomal hsa_circ_000200 as a potential biomarker and metastasis enhancer of gastric cancer via miR-4659a/b-3p/HBEGF axis. Cancer Cell Int 23: 151, 2023.
29. Livak KJ and Schmittgen TD: Analysis of relative gene expression data using real-time quantitative PCR and the 2(-Delta Delta C(T)) method. Methods 25: 402-408, 2001.
30. Malyla V, Paudel KR, Rubis G, Hansbro NG, Hansbro PM and Dua K: Extracellular vesicles released from cancer cells promote tumorigenesis by inducing epithelial to mesenchymal transition via β-catenin signaling. Int J Mol Sci 24: 3500, 2023.
31. Lin Y, Jiang H, Li J, Ren F, Wang Y, Qiu Y, Li J, Li M, Wang Y, Yang L, *et al*: Microenvironment-induced CREPT expression by cancer-derived small extracellular vesicles primes field cancerization. Theranostics 14: 662-680, 2024.
32. Gao L, Tang X, He Q, Sun G, Wang C and Qu H: Exosome-transmitted circCOG2 promotes colorectal cancer progression via miR-1305/TGF-β2/SMAD3 pathway. Cell Death Discov 7: 281, 2021.
33. Zheng R, Zhang K, Tan S, Gao F, Zhang Y, Xu W, Wang H, Gu D, Zhu L, Li S, *et al*: Exosomal circLPAR1 functions in colorectal cancer diagnosis and tumorigenesis through suppressing BRD4 via METTL3-eIF3h interaction. Mol Cancer 21: 49, 2022.
34. Guan Y, Yang W, Zhang F, Zhang L and Wang L: CircPOSTN competes with KIF1B for miR-185-5p binding sites to promote the tumorigenesis of glioma. Brain Res Bull 180: 86-96, 2022.
35. Sundar R, Nakayama I, Markar SR, Shitara K, van Laarhoven HWM, Janjigian YY and Smyth EC: Gastric cancer. Lancet 405: 2087-2102, 2025.
36. Wang XQ, Terry PD and Yan H: Review of salt consumption and stomach cancer risk: Epidemiological and biological evidence. World J Gastroenterol 15: 2204-2213, 2009.
37. Gunes-Bayir A, Guler EM, Bilgin MG, Ergun IS, Kocyigit A and Dadak A: Anti-inflammatory and antioxidant effects of carvacrol on N-methyl-N'-nitro-N-nitrosoguanidine (MNNG) induced gastric carcinogenesis in Wistar rats. Nutrients 14: 2848, 2022.
38. Li J, Chen X, Mao C, Xiong M, Ma Z, Zhu J, Li Z, Chen W, Ma H and Ye X: Epiberberine ameliorates MNNG-induced chronic atrophic gastritis by acting on the EGFR-IL33 axis. Int Immunopharmacol 145: 113718, 2025.
39. Yang E, Wang X, Gong Z, Yu M, Wu H and Zhang D: Exosome-mediated metabolic reprogramming: The emerging role in tumor microenvironment remodeling and its influence on cancer progression. Signal Transduct Target Ther 5: 242, 2020.
40. Huang S, Yan F, Qiu Y, Liu T, Zhang W, Yang Y, Zhong R, Yang Y and Peng X: Exosomes in inflammation and cancer: From bench to bedside applications. Mol Biomed 6: 41, 2025.
41. Lv X, Liu W, Zhou X, Yang Y, Zhao W, Meng L, Mu F, Zhang Z, Zhu S, Zhang S and Wang Y: Exosomes in systemic autoimmune diseases: Recent advances in diagnostic biomarkers and therapeutic applications. Int J Nanomedicine 20: 5137-5160, 2025.
42. Huang C, Li J, Xie Z, Hu X and Huang Y: Relationship between exosomes and cancer: Formation, diagnosis, and treatment. Int J Biol Sci 21: 40-62, 2025.
43. Wang J, Zhou L, Chen B, Yu Z, Zhang J, Zhang Z, Hu C, Bai Y, Ruan X Wang S, *et al*: Circular RNA circCSPP1 promotes the occurrence and development of colon cancer by sponging miR-431 and regulating ROCK1 and ZEB1. J Transl Med 20: 58, 2022.
44. O'Leary E, Jiang Y, Kristensen LS, Hansen TB and Kjems J: The therapeutic potential of circular RNAs. Nat Rev Genet 26: 230-244, 2025.
45. Pan Z, Zheng J, Zhang J, Lin J, Lai J, Lyu Z, Feng H, Wang J, Wu D and Li Y: A novel protein encoded by exosomal CircATG4B induces oxaliplatin resistance in colorectal cancer by promoting autophagy. Adv Sci (Weinh) 9: e2204513, 2022.
46. Lin J, Wang X, Zhai S, Shi M, Peng C, Deng X, Fu D, Wang J and Shen B: Hypoxia-induced exosomal circPDK1 promotes pancreatic cancer glycolysis via c-myc activation by modulating miR-628-3p/BPTF axis and degrading BIN1. J Hematol Oncol 15: 128, 2022.
47. Luo YY, Zhang HP, Huang AL and Hu JL: Association between KIF1B rs17401966 genetic polymorphism and hepatocellular carcinoma susceptibility: An updated meta-analysis. BMC Med Genet 20: 59, 2019.